Revisão: Propriedades elétricas

- Metais
- Semicondutores

Ver: (cap. 42 – Fundamentos de Física – Halliday, Resnick, Walker, vol. 4 – 6ª. Ed.)

Classificar os sólidos, do ponto de vista elétrico, de acordo com três propriedades básicas:

Concentração (densidade) de portadores de carga *n* definida como o número de portadores de carga por unidade de volume (unidades: m^{-3})

Coeficiente de temperatura da resistividade α definido pela relação:

$$\frac{1}{\rho}\frac{d\rho}{dT} = \alpha \quad \text{(unidades: } K^{-1}\text{)}$$

	Cobre	Silício
Densidade de Portadores de Carga (m^{-3})	9×10^{28}	1×10^{16}
Coeficiente de Temperatura da Resistividade (K^{-1})	$+4 \times 10^{-3}$	-70×10^{-3}

Resistividade ρ á temperatura ambiente [unidades: ohm-metro (Ω.m)]

Substância	Resistividade ($\Omega \times m$)
Cobre	1.7×10^{-8}
Ouro	2.3×10^{-8}
Alumínio	2.8×10^{-8}
Grafite	6×10^{-5}
Germânio (puro)	4.7×10^{-1}
Silício (puro)	2.1×10^{3}
Vidro	10^{10}
Mica	10^{15}
Diamante	10^{16}

Fermi energy

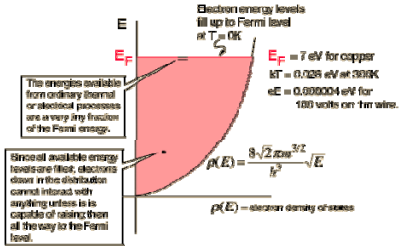

$$KE_{avg} = \left[\frac{1}{2}\overline{mv^2}\right] = \frac{3}{2}kT$$

• The Fermi energy is the maximum energy occupied by an electron at 0K. By the Pauli exclusion principle, we know that the electrons will fill all available energy levels, and the top of that "Fermi sea" of electrons is called the Fermi energy or Fermi level. One of the remarkable things about the Fermi energy is how large it is compared to the energies which electrons could gain by ordinary physical interactions with their environment.

• The amount of energy available as a result of the temperature of the material is on the order of the average thermal energy, for which kT= .026 eV at 300K is a representative number. This is very small compared to the Fermi energy of 7 eV for copper. This tells us that that thermal energy can interact with only a tiny fraction of the electrons (roughly .026/7 or about 0.4% of the energy range), since the overwhelming majority of the electrons are separated from the top of the Fermi sea by much more than thermal energy. This correlates well with the observation that electrons do not contribute significantly to the specific heat of solids at ordinary temperatures. Only at very low temperatures does the electron specific heat become significant.

METAIS

Diagrama de Bandas

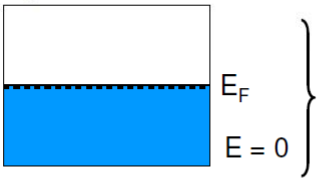

Banda Parcialmente Preenchida

- E_F = nível de Fermi = energia de Fermi ⟶ definido para T = 0 K
- elétrons que ocupam banda parcialmente preenchida ⟶ elétrons de valência
- Cobre:

E_F = 7,0 eV , v_F = 0,0052 c = 1,6 x 10^6 m/s (vel. dos elétrons no nível de Fermi)

para T= 0 K

O que acontece se aumentarmos a temperatura??

Energia Térmica (kT)

- Elétrons próximos ao nível de Fermi irão para níveis vagos acima do nível de Fermi continuarão aprisionados nesta banda
- Distribuição de elétrons não difere muito da distribuição no zero absoluto
- *Energia Térmica = kT energia cedida ao elétron* através do aumento de temperatura
- (k = constante de Boltzman = 8,62 x 10^{-5} eV/K)
- T=1000 K (727 ^{o}C) kT = 0,086 eV
- Pouca alteração na energia do elétron

Condução elétrica num metal: Resistividade ρ

Expressão baseada no modelo de elétrons livres (gás de elétrons) – elétrons de condução

- Aplica-se um campo elétrico E ⇒ força F aplicada em cada elétron $F = -eE$
- Tempo Δt ⇒ aumento de Δv na velocidade dos elétrons de condução no sentido –E
  - ⇒ variação na energia dos elétrons
  - ⇒ ocupam outros níveis vagos
- Velocidade dos elétrons não cresce sem limites
  - ⇒ colisões com vibrações térmicas da rede limita a velocidade
  - ⇒ chega a um valor constante ⇒ corrente constante
  - ⇒ tempo para que isto ocorra: tempo de relaxação τ

$$\rho = \frac{m}{ne^2\tau}$$

m = massa do elétron; e = carga do elétron;

n = concentração de portadores de cargas (nº de elétrons de condução por volume.

METAIS: como varia a resistividade com o aumento da temperatura?

$$\rho = \frac{m}{ne^2\tau}$$

- Concentração de portadores de carga (n) não aumenta muito, por causa dos processos de colisão;
- Tempo de relaxação τ diminui bastante com o aumento no número de colisões, mais rápido se chega a uma corrente constante.

ρ AUMENTA com a temperatura

$$\frac{1}{\rho}\frac{d\rho}{dT} = \alpha$$

α = coeficiente de temperatura da resistividade é POSITIVO!

Como se calcula o número de elétrons de condução (N_{ec}) num sólido?

$$N_{ec} = N_{átomos} \times N_{elétrons\ de\ valência/átomo}$$

$$n = \frac{N_{ec}}{volume\ da\ amostra}$$

$$n = \frac{N_{átomos} \times N_{elétrons\ de\ valência/átomo}}{volume\ da\ amostra}$$

Concentração de portadores de carga

$$N_{átomos} = \frac{M_{amostra}}{massa\ atômica} = \frac{massa\ específica \times volume}{massa\ atômica}$$

$$massa\ atômica = \frac{massa\ molar}{N_A}$$

$N_A = 6{,}02 \times 10^{23}\ mol^{-1}$

Estudo Quantitativo da Eletricidade num Metal

1) Contagem de Estados Quânticos:
   para 1 átomo: *2 (2l + 1)*
   para N átomos num sólido: ??
2) Contagem dos Estados em T = 0 K
3) Cálculo da Energia de Fermi
4) Contagem dos Estados em T > 0 K

1) Contagem de estados quânticos:

N átomos: método estatístico

Em vez de perguntarmos: "qual a energia do estado? "

Perguntamos: "quantos estados (por unidade de volume) tem energia entre E e E + dE? "

- Um cristal com 10^{23} átomos origina um número muito grande de níveis de energia. Muitos dos quais são denenerados (= Energia)
- A densidade de estados ***N*(E)** é a medida de estados disponíveis com a mesma energia, por unidade de volume

Densidades de Estados

$$N(E) = \frac{8\pi}{h^3}\left(2m^3E\right)^{1/2}$$

Densidade de Estados

$$N(E) = \frac{8\pi}{h^3}\left(2m^3E\right)^{1/2}$$

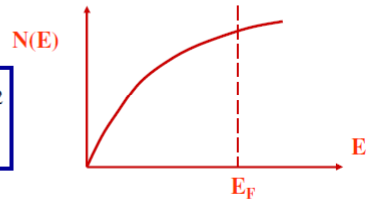

Não depende da forma, tamanho e material da amostra

É função apenas da energia!!

2) Contagem de estados em T = 0 K:

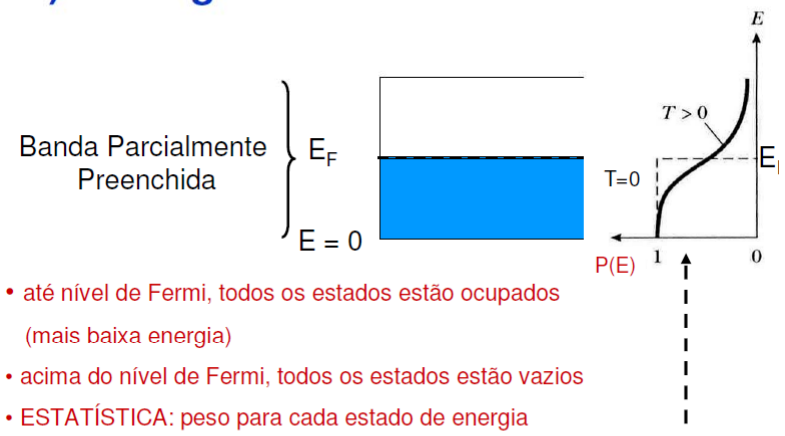

- até nível de Fermi, todos os estados estão ocupados (mais baixa energia)
- acima do nível de Fermi, todos os estados estão vazios
- ESTATÍSTICA: peso para cada estado de energia

P(E) ⇒ função probabilidade
- = 1 certeza que o estado está ocupado
- = 0 certeza que o estado está vazio

Densidade de Ocupação de Estados

Nº de estados ocupados por unidade de volume

$$N_o(E) = N(E)\,P(E)$$

N° de estados não ocupados por unidade de volume (densidade de estados)

$$N(E) = \frac{8\pi}{h^3}(2m^3E)^{1/2}$$

Probabilidade de ocupação de um estado

P(E) = 1 ou = 0

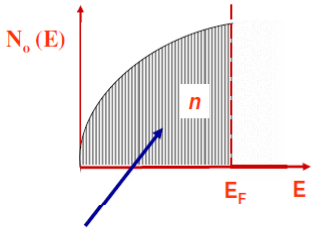

$$n = \int_0^{E_F} N_o(E)\,dE = \int_0^{E_F} N(E)P(E)\,dE$$

n = N° de elétrons de condução por unidade de volume num metal

$$n = \int_0^{E_F} N(E)\,dE$$

Em T = 0 K os elétrons de condução ocupam todos os estados de energia até o nível de Fermi

3) Cálculo da Energia de Fermi

$$n = \int_0^{E_F} N(E)dE = \int_0^{E_F} \frac{8\pi}{h^3}(2m^3E)^{1/2}dE = \frac{8\pi}{h^3}(2m^3)^{1/2}\left[\frac{E^{3/2}}{3/2}\right]_0^{E_F}$$

$$n = \frac{16\pi}{3h^3}(2m^3)^{1/2}E_F^{3/2}$$

isolando E_F, temos:

$$A = 3{,}65\times10^{-19}\ (m^2eV)$$

$$E_F = \left(\frac{3}{16\sqrt{2}\pi}\right)^{2/3}\frac{h^2}{m}n^{2/3} = \frac{0{,}121\cdot h^2}{m}n^{2/3} = An^{2/3}$$

m = massa do elétron

Sabendo n (n° de elétrons de condução por volume) calcula-se E_F

4) Contagem de estados para T > 0 K

Como fica a função probabilidade P(E)?

Temos a distribuição de probabilidades de Fermi-Dirac que representa a probabilidade de ocupação de um estado de com energia E.

$$P(E) = \frac{1}{e^{(E-E_F)/kT} + 1}$$

Em T = 0 K temos:

- para $E < E_F \Rightarrow (E - E_F)/kT \Rightarrow -\infty$ $\Rightarrow e^{-\infty} = 0 \Rightarrow P(E) = 1$
- para $E < E_F \Rightarrow (E - E_F)/kT \Rightarrow +\infty$ $\Rightarrow e^{+\infty} = \infty \Rightarrow P(E) = 0$

4) Contagem de estados para T > 0 K

$$P(E) = \frac{1}{e^{(E-E_F)/kT} + 1}$$

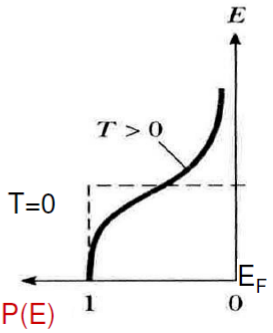

$$n = \int_0^E N_o(E)\,dE = \int_0^E N(E)\,P(E)\,dE$$

Comparando ocupação de estados para:

T = 0 K **T > 0 K**

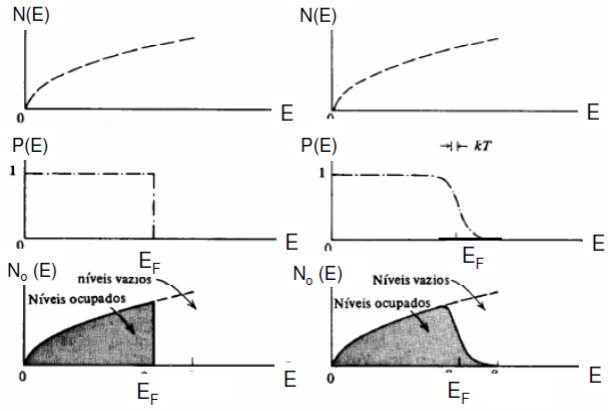

SEMICONDUTORES

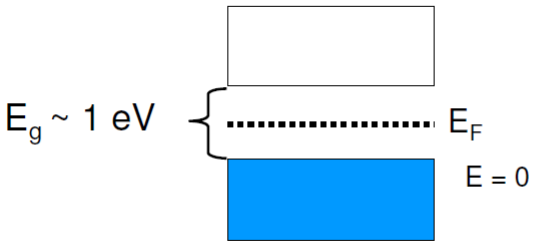

Elétron pode saltar da banda de valência para a banda de condução por simples agitação térmica

Concentração de portadores de carga:

Para metais: elétrons de condução (= n º de elétrons de valência por átomo)

n_{Cu}= 9 x 10^{28} (m^{-3}) em temperatura ambiente

Para semicondutores: portadores de carga surgem apenas por agitação térmica

Elétrons saltam da banda de valência para a banda de condução, gerando

espaços vazios na banda de valência

BURACOS

Semicondutor Intrínseco

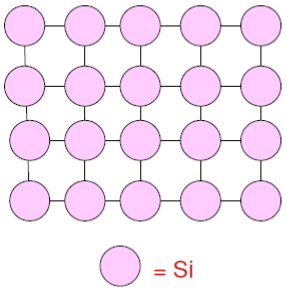

= Si

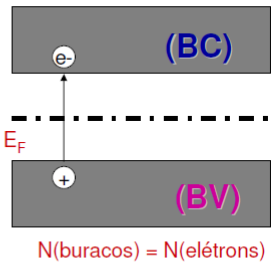

N(buracos) = N(elétrons)

2 tipos de portadores de carga:

Elétrons na banda de condução (BC)

Buracos na banda de valência (BV)

Semiconductors

B	C	N	O
Al	Si	P	S
Ga	Ge	As	Se
In	Sn	Sb	Te

http://worldwatts.com/silicon_semiconductor.html

Condução elétrica em semicondutores:

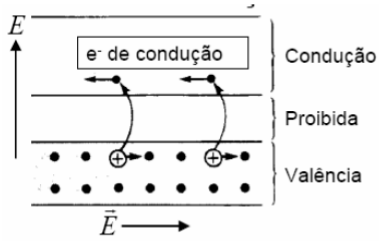

Um campo elétrico aplicado a um semicondutor produz condução elétrica devido ao movimento dos e^- na banda de condução, bem como dos buracos na banda de valência. No caso dos buracos, o movimento também se deve aos e^-, que, devido ao campo, ocupam sucessivamente a vacância deixada pelo e^- promovido à banda de condução, fazendo com que a vacância se desloque no sentido oposto.

SEMICONDUTORES: como varia a resistividade com o aumento da temperatura?

$$\rho = \frac{m}{ne^2\tau}$$

- Concentração de portadores de carga (n) aumenta rapidamente com a temperatura (elétrons e buracos);
- Tempo de relaxação τ tem uma diminuição pequena frente ao aumento de (n)

ρ DIMINUI com a temperatura

$$\frac{1}{\rho}\frac{d\rho}{dT} = \alpha$$

α = coeficiente de temperatura da resistividade é NEGATIVO!

$\alpha_{Si} = -\ 70 \times 10^{-3}\ K^{-1}$

RESUMO:

Propriedade	*Metais (M)*	*Semicondutores (S)*	*Observações*
Portadores de carga (n)	Elétrons de condução	Elétrons + Buracos	$n_M > n_S$
Resistividade $\rho = \frac{m}{ne^2\tau}$	Pequena	Grande	$\rho_M < \rho_S$
Coeficiente de temperatura da resistividade $\frac{1}{\rho}\frac{d\rho}{dT} = \alpha$	$\frac{d\rho}{dT} > 0 \Rightarrow \alpha > 0$ • τ diminui com T • n independe de T	$\frac{d\rho}{dT} < 0 \Rightarrow \alpha < 0$ • τ diminui pouco comparado ao aumento de n com T • n aumenta de T	$\alpha_M > 0$ $\alpha_S < 0$

Dopagem de Semicondutores

Objetivo: aumentar a condutividade do SC pela adição de uma pequena quantidade de outro material, denominado de ***dopante***

Semicondutor Intrínseco

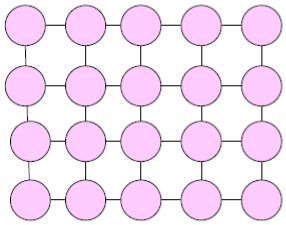

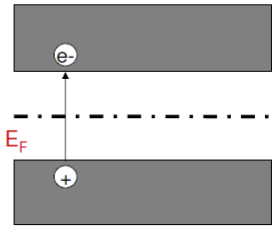

n(buracos) = n(elétrons)

= Si Valência do Si +4

Semicondutor Extrínseco Tipo p (positivo): Portadores majoritários: buracos (BV)

→Dopagem substitucional: 1 átomo de Si é substituído por um átomo de B (valência +3)

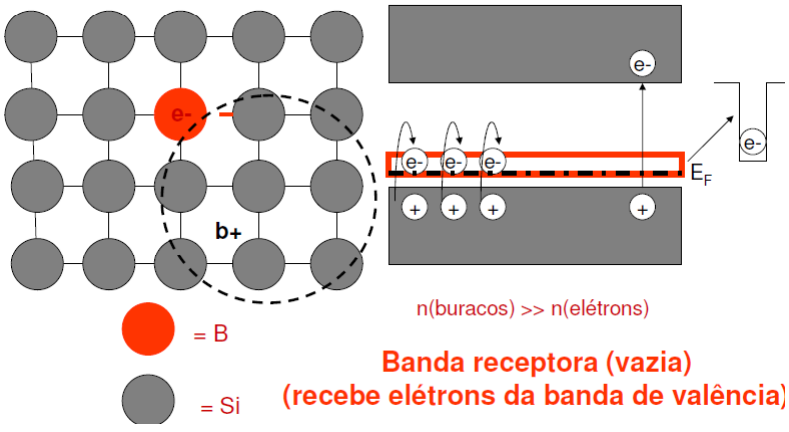

n(buracos) >> n(elétrons)

= B

= Si

Banda receptora (vazia)
(recebe elétrons da banda de valência)

Semicondutor Extrínseco Tipo n (negativo): Portadores majoritários: elétrons (BC)

→Dopagem substitucional: 1 átomo de Si é substituído por 1 átomo de P (valência +5)

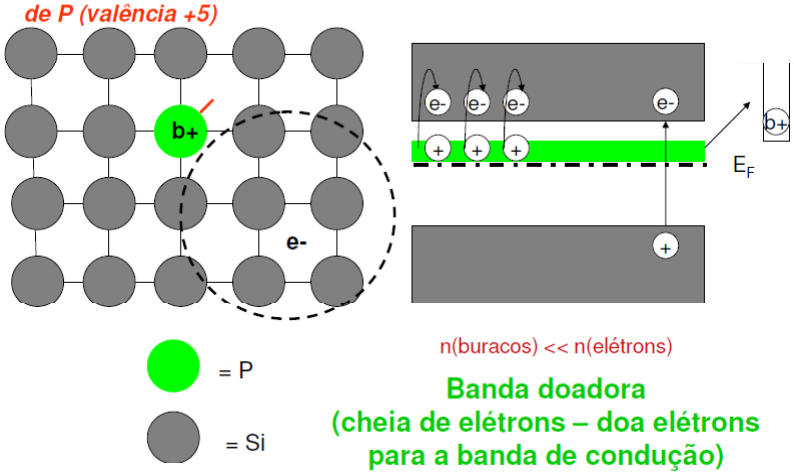

n(buracos) << n(elétrons)

Banda doadora (cheia de elétrons – doa elétrons para a banda de condução)

This crystal has been doped with a pentavalent impurity.

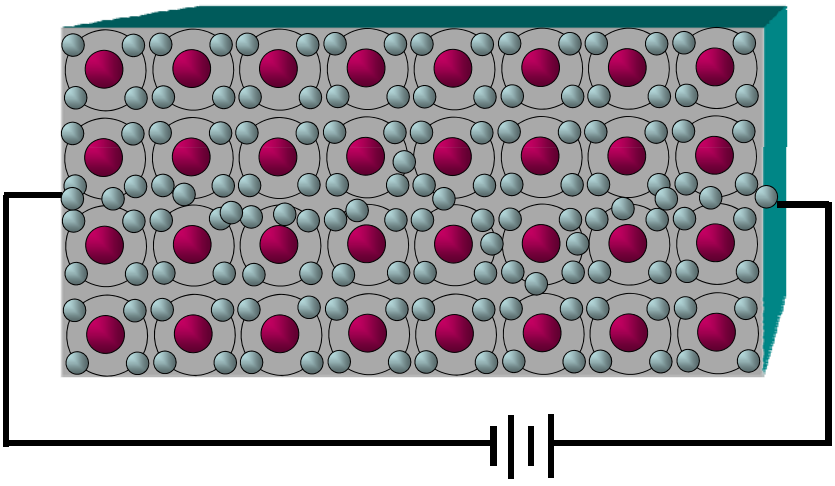

The free electrons in n type silicon support the flow of current.

This crystal has been doped with a trivalent impurity.

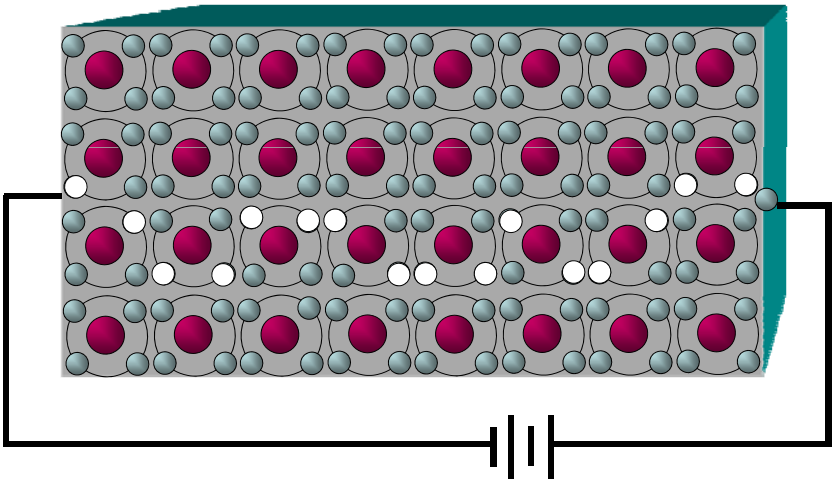

The holes in p type silicon contribute to the current.

Note that the hole current direction is opposite to electron current so the electrical current is in the same direction

Supercondutividade

- Supercondutividade - é uma propriedade física, de característica intrínseca de certos materiais, quando resfriados a temperaturas extremamente baixas, tendem a conduzir corrente elétrica sem resistência nem perdas.

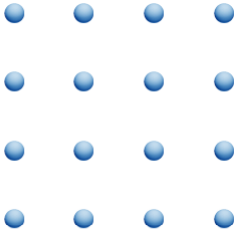

Walther Meissner e Robert Ochsenfeld concluíram que supercondutores quando colocados imersos em um campo magnético externo e resfriados abaixo da sua temperatura de transição, tendem a ejetar todo o campo magnético aplicado. Esse fenômeno é chamado de Efeito Meissner, mas não se resume apenas na ejeção do campo magnético por parte do supercondutor, pois na verdade o campo externo tende a penetrar o supercondutor mas apenas até uma certa profundidade definida por um parâmetro λ, denominado parâmetro de penetração de London, decaindo exponencialmente a zero na maior parte do material supercondutor. O efeito Meissner é uma característica primordial da supercondutividade, e para a maioria dos supercondutores λ é da ordem de 100 nm.

Nanotubos de Carbono

Referências: Nanotubos de Carbono

. "High Resolution TEM Observations of Single-Walled Carbon Nanotubes", Tara Spires and R. Malcolm Brown, Jr. Department of Botany, The University of Texas at Austin, Austin,Tx., 78713 [1996]

Location: http://www.botany.utexas.edu/facstaff/facpages/mbrown/ongres/tspires/nano.htm

2. "Crystalline Ropes of Metallic Carbon Nanotubes", Science 273, 483 (1996), Andreas Thess, Roland Lee, Pavel Nikolaev, Hongjie Dai, Pierre Petit, Jerome Robert, Chunhui Xu, Young Hee Lee, Seong Gon Kim, Andrew G. Rinzler, Daniel T. Colbert, Gustavo Scuseria, David Tománek, John E. Fischer, Richard E. Smalley

Smalley's Website: http://cnst.rice.edu/reshome.html

Location: http://cnst.rice.edu/ropes.html

3. Energetics, Structure, Mechanical and Vibrational Properties of Single Walled Carbon Nanotubes (SWNT)", by Guanghua Gao, Tahir Cagin*, and William A. Goddard III, [1997]

Location: http://www.wag.caltech.edu/foresight/foresight_2.html

4. "Fractional Quantum Conductance in Carbon Nanotubes", cond-mat/9908154, Phys. Rev. Lett. 84, 1974 (2000), Stefano Sanvito, Young-Kyun Kwon, David Tománek, and Colin J. Lambert.

Location: http://www.pa.msu.edu/cmp/csc/eprint/prlxtsp/prlxtsp.html

5. Stefan Frank et al., Science 280 1744 (1998)

Nanotubes Lab: http://electra.physics.gatech.edu/group/labs/tubelab.html

6. "Thermal Conductivity of Carbon Nanotubes", by Jianwei Che, Tahir Cagin, and William A. Goddard III

Location: http://www.foresight.org/Conferences/MNT7/Papers/Che/index.html

7. "Young's Modulus of Single-Walled Nanotubes", E. DUJARDIN, AND T. W. EBBESEN, AND A. KRISHNAN, AND P. N. YIANILOS, AND, M. M. J. TREACY, Physical Review B 58(20) pp. 14013-14019, 15/Nov 1998.

Location: http://www.intermemory.net/pny/papers/youngs/main.html

8. "Nanotubes: Mechanical and Spectroscopic Properties" .5em E. Hernández1 and Angel Rubio2 [1999]

1 School of Chemistry, Physics and Environmental Science,University of Sussex, Brighton BN1 9QJ, England UK

2 Departamento de Física Teórica, Universidad de Valladolid, E-47011 Valladolid, Spain.

Location: http://www.fam.cie.uva.es/~arubio/psi_k/node5.html

9. "Physics News Update, The American Institute of Physics Bulletin of Physics News, Number 279 (Story #2)", July 15, 1996 by Phillip F. Schewe and Ben Stein.

Location: http://www.aip.org/enews/physnews/1996/split/pnu279-2.htm

10. "Carbon Nanotubes", Anthony Kendall, Thomas A. Adams II, and Elizabeth Pfaff [1999]

Location: http://www.msu.edu/~pfaffeli

Referências: Nanotubos de Carbono

11. "Richard E Smalley's Homepage", Richard Smalley

Location: http://cnst.rice.edu/reshome.html

Image Gallery: http://cnst.rice.edu/pics.html

13. David Tomànek

Personal Web Site: http://www.pa.msu.edu/~tomanek/tomanek.html

14. Science and Application of Nanotubes, Edited by D. Tomànek and R.J. Enbody, Kluwer Academic / Plenum Publishers, New York, 2000

15. J. Hone, M. Whitney, A. Zettle, Synthetic Metals, 103 2498 (1999)

16. "Unusually High Thermal Conductivity of Carbon Nanotubes", Savas Berber, Young-Kyun Kwon, and David Tomànek, Phys. Rev. Lett. 84 (2000)

17. Z. W. Pan; S. S. Xie; B. H. Chang; C. Y. Wang; L. Lu; W. Liu; W. Y. Zhou; W. Z. Li; L. X. Qian, Nature Volume 394 Number 6694 Page 631 - 632 (1998)

18. Min-Feng Yu, Bradley S. Files, Sivaram Arepalli, Rodney S. Ruoff, Phys. Rev. Lett. 84, 5552 (2000).

19. C. Dekker, "Carbon Nanotubes as Molecular Quantum Wires", Physics Today, p22, May (1999)

20. "Electronic and Mechanical Properties of Carbon Nanotubes", L. Forró, J.-P. Salvetat, J.-M. Bonard, R. Basca, N. H. Thomson, S. Garaj, L. Thien-Nga, R. Gaál, A. Kulik, B. Ruzicka, L. Degiorgi, A. Bachtold, C. Schönenberger, S. Pekker, K. Hernadi, Science and Application of Nanotubes, p297 (see ref14)

21. "TEM & SEM Images of Nanotubes", Zettle Research Group

Location: http://www.physics.berkeley.edu/research/zettl/projects/imaging.html

22. S. Iijima, Nature, 354 56 (1991)

23. Jeroen W. G. Wilder; Liesbeth C. Venema; Andrew G. Rinzler; Richard E. Smalley; Cees Dekker; Nature 391, 6662, 59-62 (1998)

24. Teri Wang Odom; Jin-Lin Huang; Philip Kim; Charles M. Lieber; Nature 391, 6662, 62-64 (1998).

Estruturas de Carbono

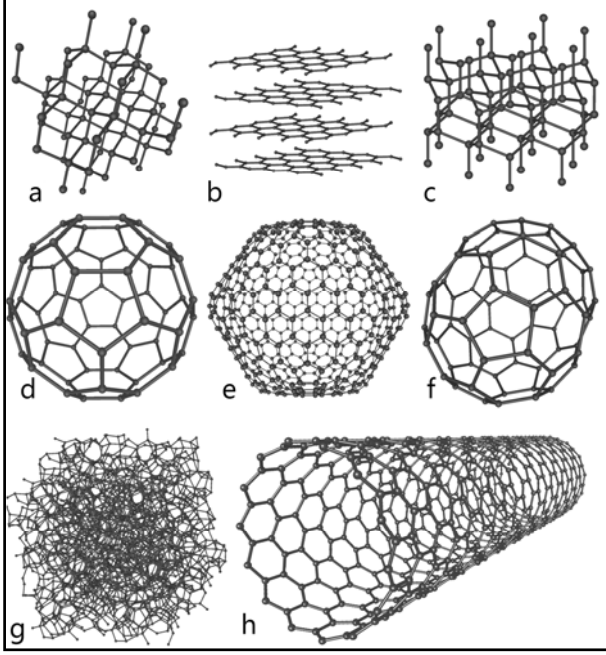

a) Diamante
b) Grafite
c) Lonsdaleite
d) C60
e) C540
f) C70
g) Carnono Amorfo
h) Nanotubo de Carbono (single-walled)

Estruturas de Carbono

Alotropia

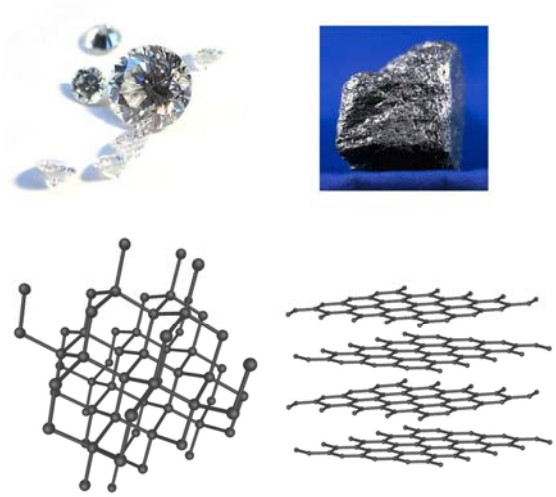

Carbono: Hibridização

✓ **Hibridização:** formação de orbitais híbridos.

✓ **subníveis atômicos: s** e **p** se misturam formando orbitais híbridos sp, sp^2 e sp^3.

✓ **Sobreposição de orbitais semipreenchidos**

✓ Explica a formação de algumas **ligações** e disposição **geométrica**

Carbono: Hibridização

C (z = 6) = $1s^2$ $2s^2$ $2p^2$

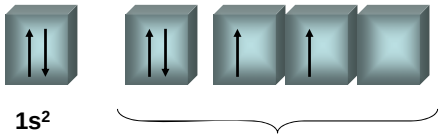

$1s^2$ **$2s^2$ $2p^2$**

Carbono: Hibridização

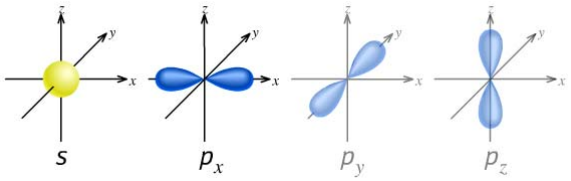

Carbono: Hibridização

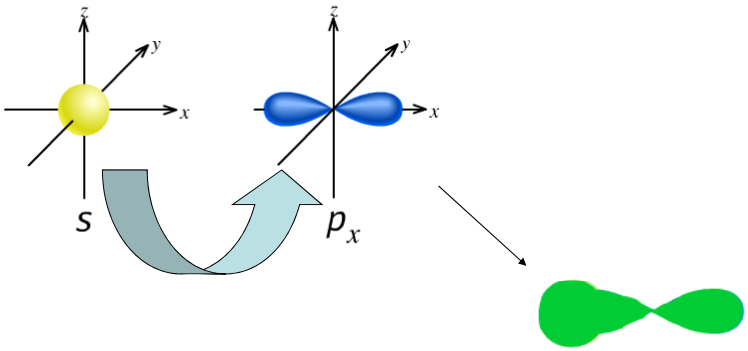

Carbono: Hibridização

Carbono: Hibridização

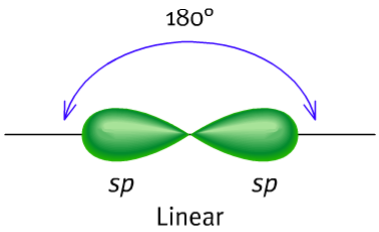

Carbono: Hibridização

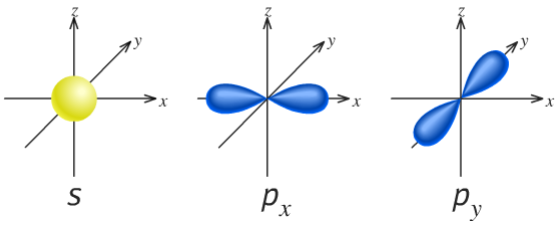

Carbono: Hibridização

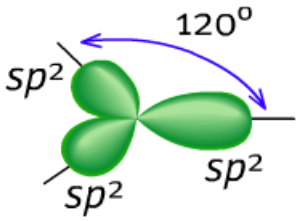

Trigonal Planar

Hibridização

Pure atomic orbitals of central atom	Hybridization of the central atom	Number of hybrid orbitals	Shape of hybrid orbitals
s,p	sp	2	Linear
s,p,p	sp^2	3	Trigonal Planar
s,p,p,p	sp^3	4	Tetrahedral
s,p,p,p,d	sp^3d	5	Trigonal Bipyramidal
s,p,p,p,d,d	sp^3d^2	6	Octahedral

Carbono: Hibridização

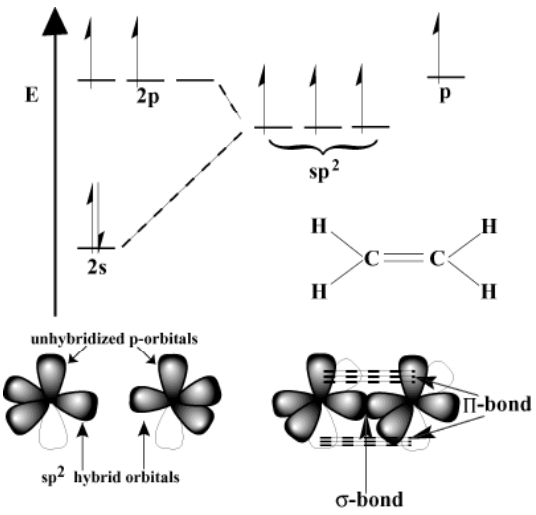

Carbono: Hibridização

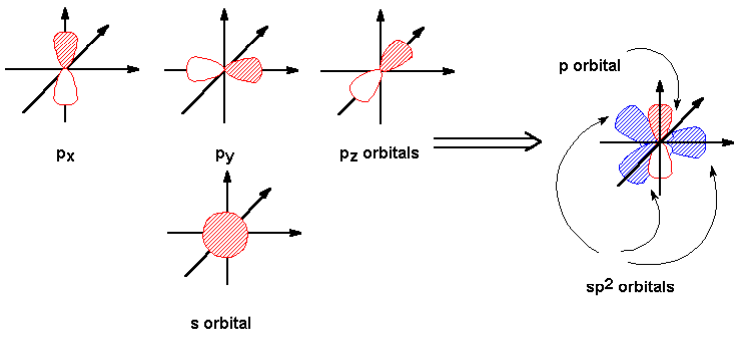

Nanotubos de Carbono

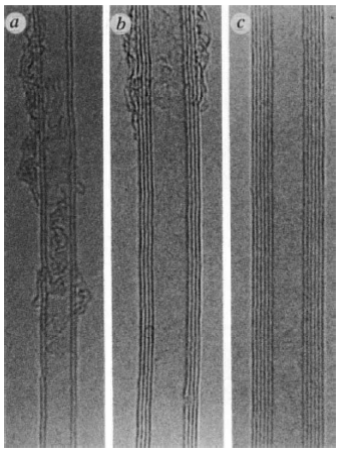

- **single wall (SWNT)**
- **multiple walls (MWNT)**

Nanotubos de Carbono

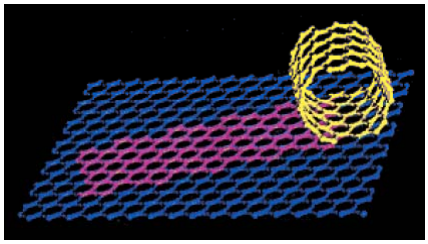

Dependendo como o grafeno é “enrolado” podemos obter diferentes formas de nanotubos.

Single-Wall Nanotubes SWNTs

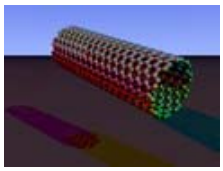

Armchair (*n*,*n*)

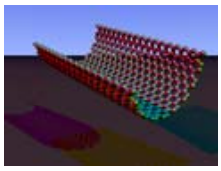

The chiral vector is bent, while the translation vector stays straight

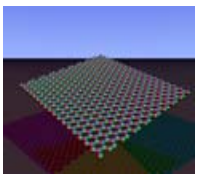

Graphene nanoribbon

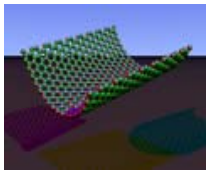

The chiral vector is bent, while the translation vector stays straight

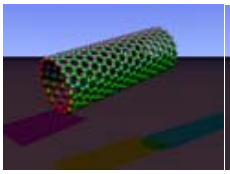

Zigzag (*n*,0)

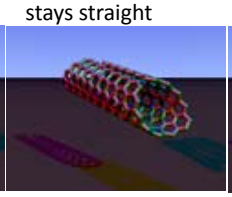

Chiral (*n*,*m*)

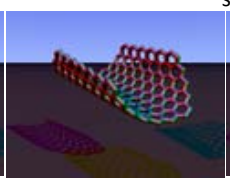

n and *m* can be counted at the end of the tube

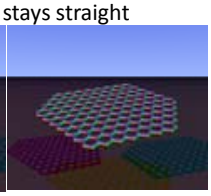

Graphene nanoribbon

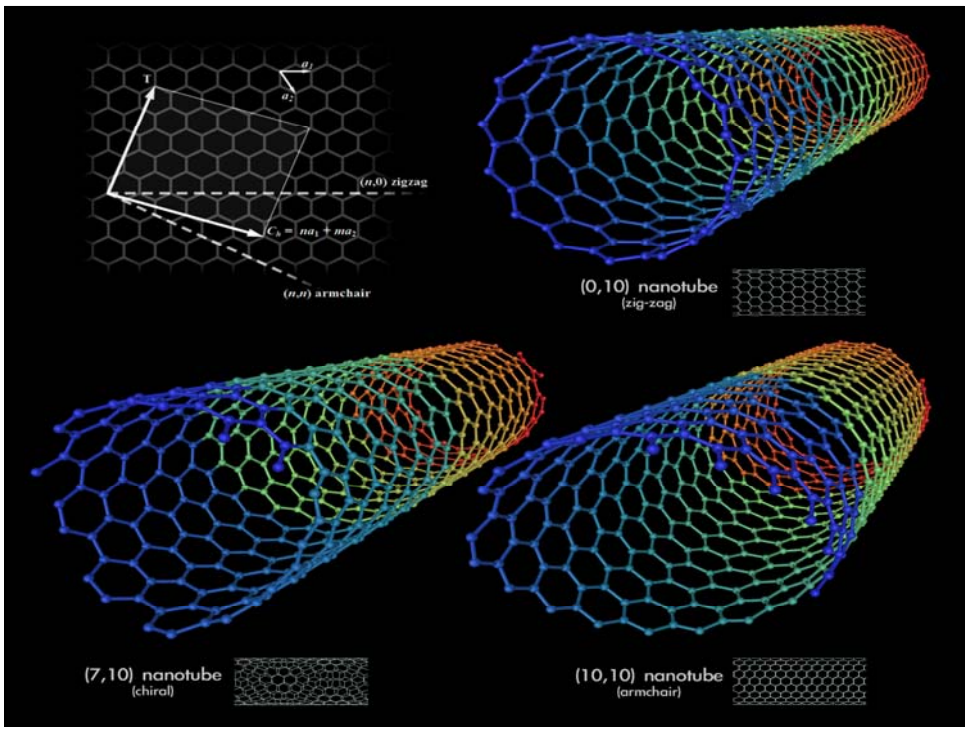

Nanotubos de Carbono

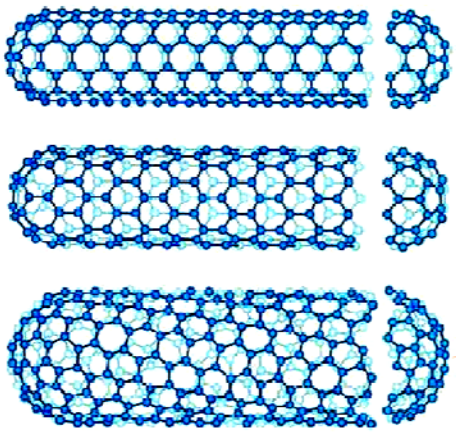

SWNT armchair

SWNT zig-zag

SWNT quiral

Folha de Grafeno e Nanotubos de Carbono

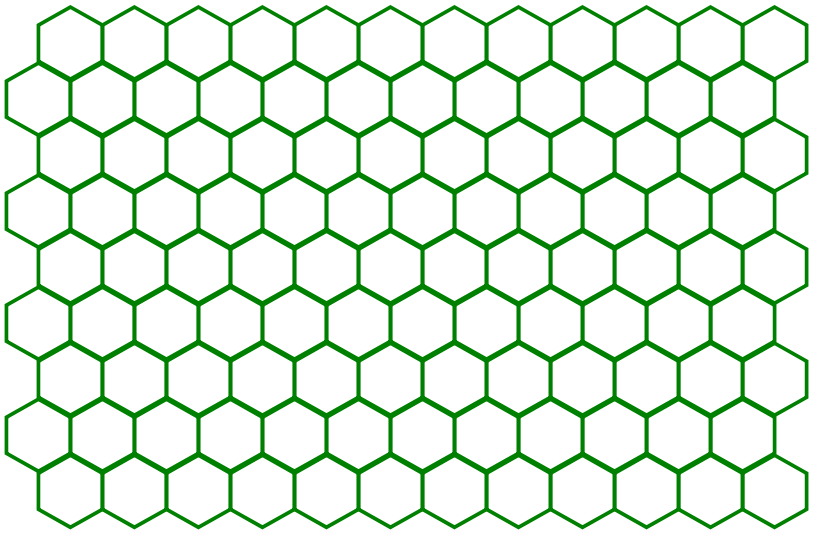

Nanotubos de Carbono

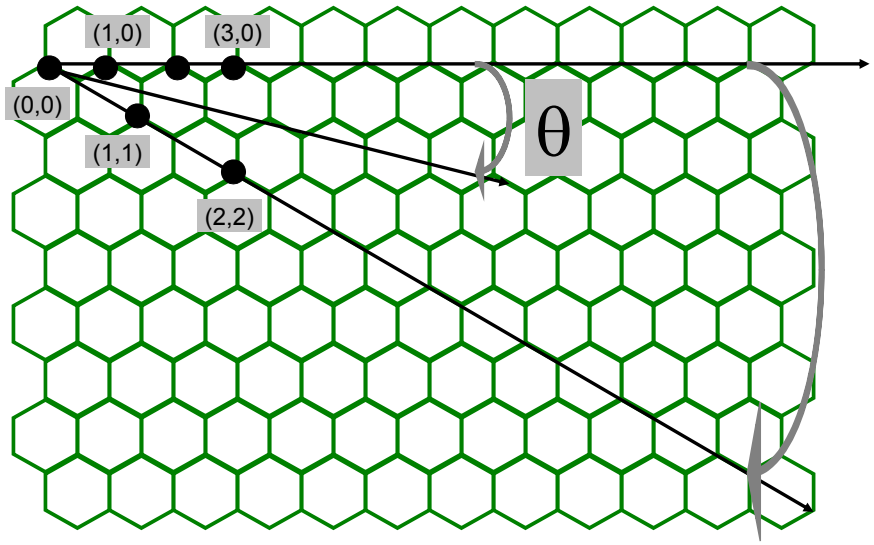

Folha de Grafeno e Nanotubos de Carbono

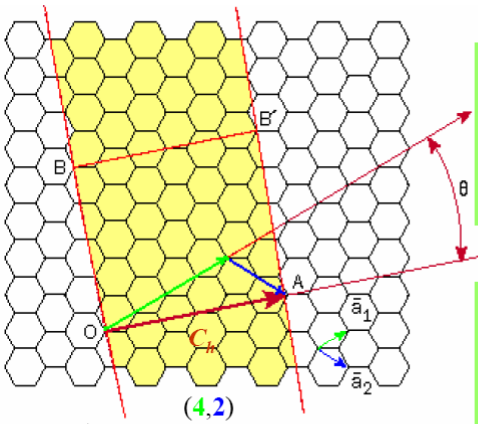

Diâmetro do tubo, d_t

$$\left|\vec{C}_h \cdot \vec{C}_h\right| = \pi d_t$$

$$d_t = \frac{\sqrt{3}a_{C-C}}{\pi}(n^2 + m^2 + nm)^{1/2}$$

Ângulo quiral, θ

$$\vec{C}_h \cdot \vec{a}_1 = \left|\vec{C}_h\right|\left|\vec{a}_1\right|\cos\theta$$

$$\theta = \cos^{-1}\left(\frac{n + \frac{m}{2}}{\sqrt{(n^2 + m^2 + nm)}}\right)$$

Folha de Grafeno e Nanotubos de Carbono

$$\theta = \cos^{-1}\left(\frac{n+\frac{m}{2}}{\sqrt{(n^2+m^2+nm)}}\right)$$

$i) m = 0$

$$\theta = \cos^{-1}\left(\frac{n}{\sqrt{(n^2)}}\right) \Rightarrow \theta = 0^0$$

$ii) n = m$

$$\theta - \cos^{-1}\left(\frac{3n/2}{\sqrt{(3n^2)}}\right) - \cos^{-1}\left(\frac{\sqrt{3}}{2}\right) \rightarrow \theta - 30^0$$

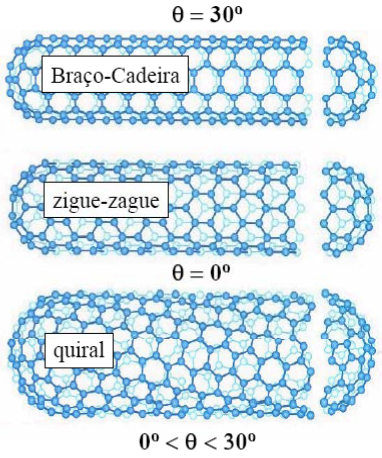

Nanotubos de Carbono: Armchair

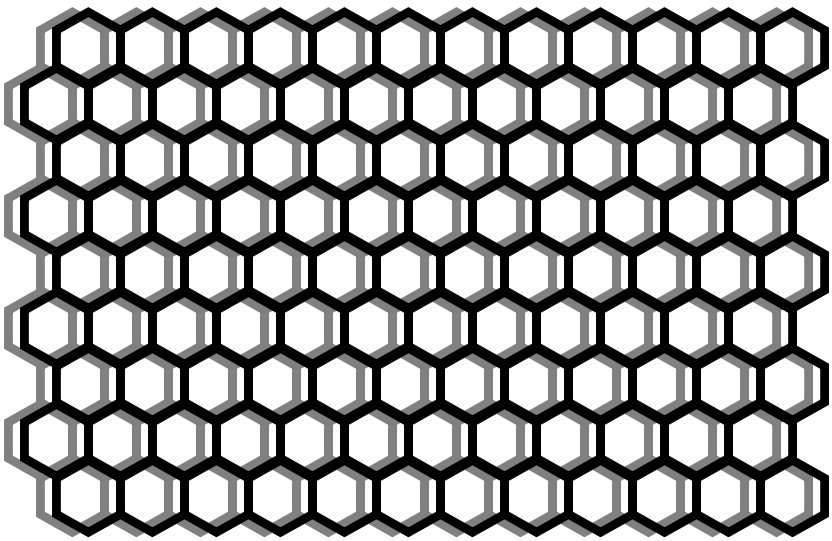

Nanotubos de Carbono: zigzag

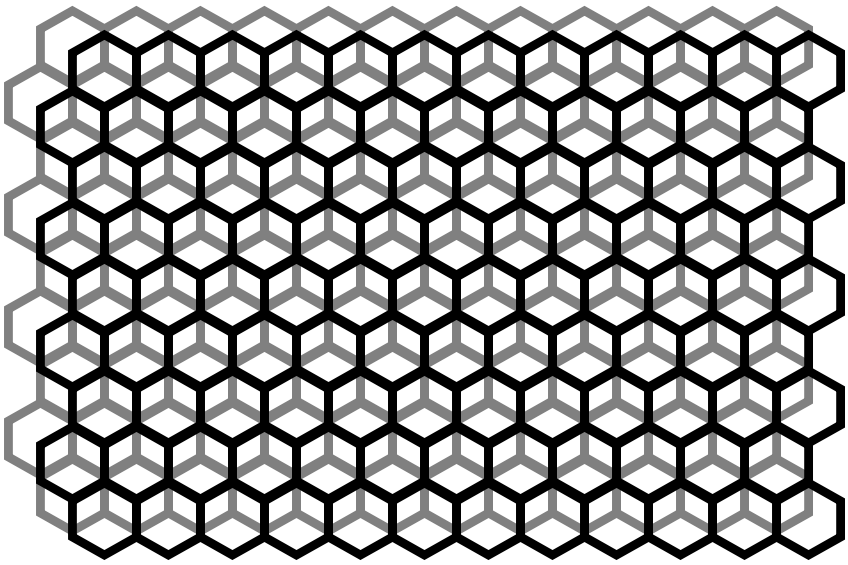

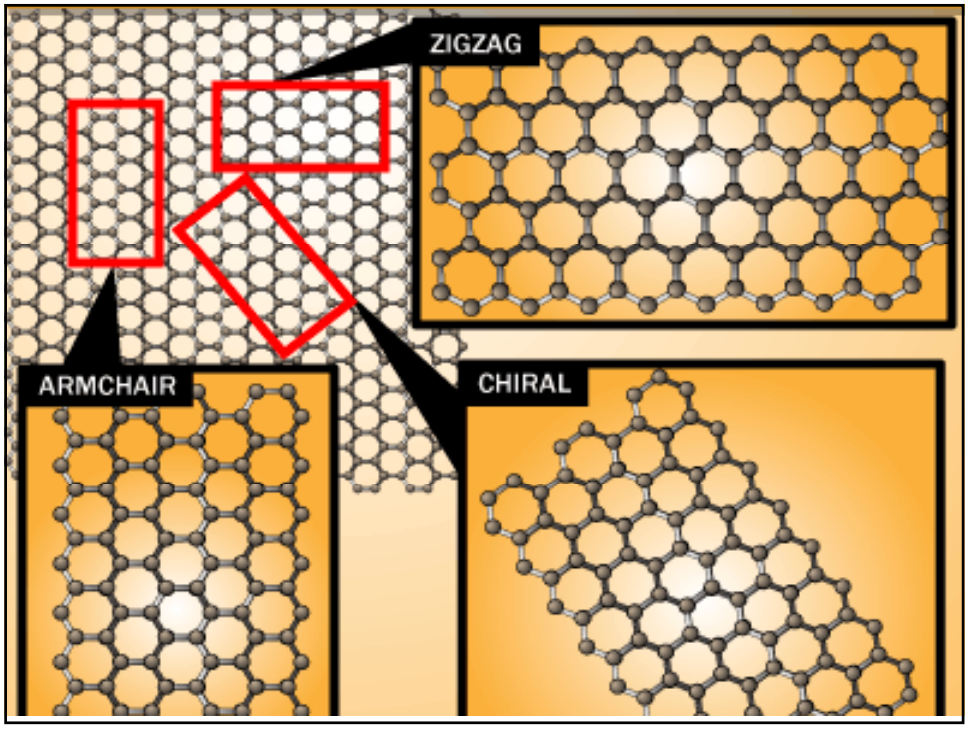

Nanotubos de Carbono

Ângulo quiral

$$\theta = \arctan\left(\frac{-\sqrt{3}m}{2n+m}\right),\ 0 \le \theta \le 30^{0}$$

Nanotubos de Carbono

- ✓ **armchair: caráter metálico**
- ✓ **n-m = 3k ➔ semicondutores ➔ baixo band gap**
- ✓ **SWNT com diâmetro entre 0,6 e 1,6 apresentam band gap entre 0,4 e 1,0eV**
- ✓ **MWNT apresentam interação fraca entre os tubos: van der Waals**

Nanotubos de Carbono: Propriedades

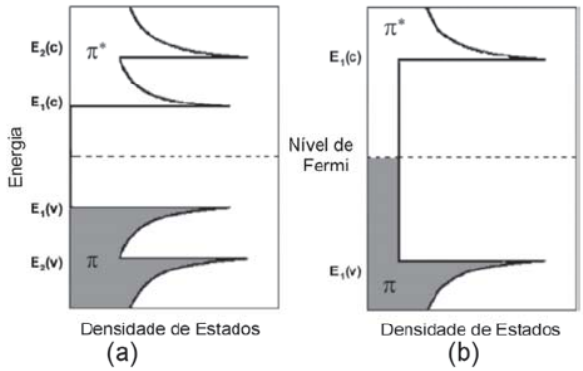

Densidade de estados eletrônicos para SWNTs semicondutores (a) e metálicos (b). Os estados preenchidos (orbitais π) estão localizados abaixo do nível de Fermi e os estados vazios (orbitais π) acima do nível de Fermi*

Nanotubos de Carbono: Propriedades

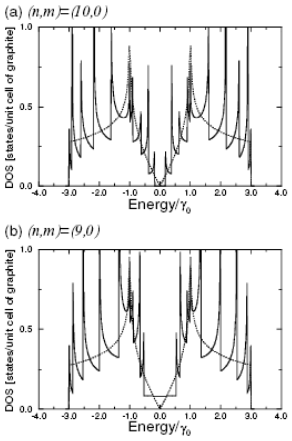

Electronic 1D density of states per unit cell of a 2D graphene sheet for two $(n,0)$ zigzag nanotubes: (*a*) the $(10,0)$ nanotube which has semiconducting behaviour, (*b*) the $(9,0)$ nanotube which has metallic behaviour. Also shown in the figure is the density of states for the 2D graphene sheet (dotted line)

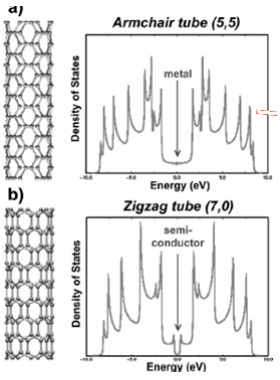

Fonte: *SAITO, R., DRESSELHAUS, G., and DRESSELHAUS,M. S., 1993, J. appl. Phys., 73, 494.*

Síntese de Nanotubos de Carbono

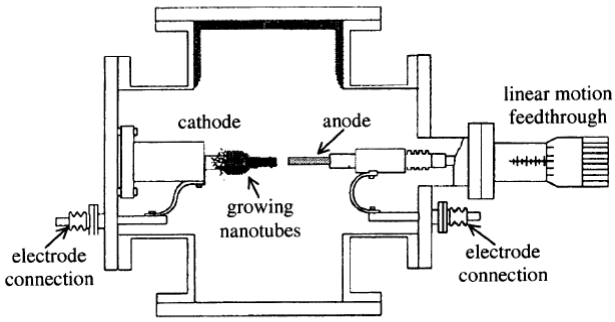

Schematic illustration of the arc-discharge technique

Fonte: *E.T. Thostenson et al. / Composites Science and Technology 61 (2001) 1899–1912*

Síntese de Nanotubos de Carbono

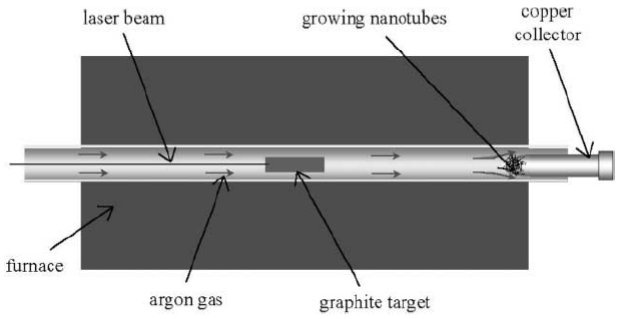

Schematic of the laser ablation process

Fonte: *E.T. Thostenson et al. / Composites Science and Technology 61 (2001) 1899–1912*

Synthesis of Carbon Nanotube

1 Laser Ablation – Experimental Devices

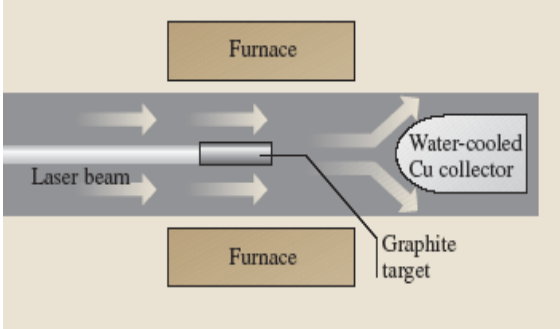

Sketch of an early laser vaporization apparatus

- graphite pellet containing the catalyst put in an inert gas filled quartz tube;
-oven maintained at a temperature of 1,200 °C;
-energy of the laser beam focused on the pellet;
-vaporize and sublime the graphite

The carbon species are there after deposited as soot in different regions: water-cooled copper collector, quartz tube walls.

2 Synthesis with CO_2 laser

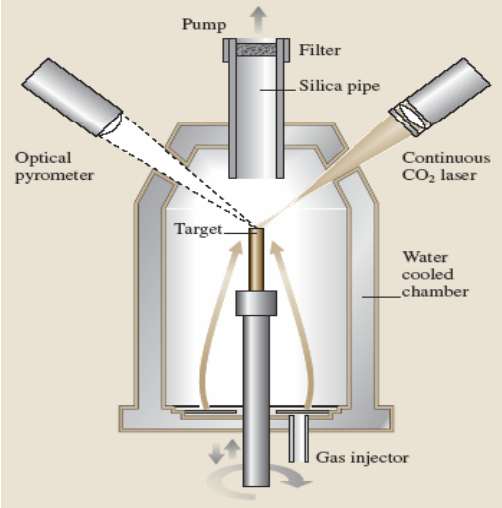

Fig. 3.10 Sketch of a synthesis reactor with a continuous CO_2 laser device

Vaporization of a target at a fixed temperature by a continuous CO_2 laser beam (λ = 10.6μm). The power can be varied from 100Wto 1,600 W.

The synthesis yield is controlled by three parameters: the cooling rate of the medium where the active, secondary catalyst particles are formed, the residence time, and the temperature (in the 1,000–2,100K range) at which SWNTs nucleate and grow.

3 Electric-Arc Method – Experimental Devices

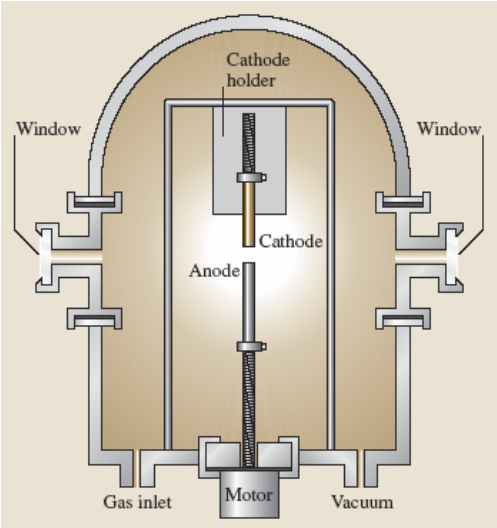

Sketch of an electric arc reactor. It consists of a cylinder of about 30 cm in diameter and about 1m in height.

After the triggering of the arc between two electrodes, a plasma is formed consisting of the mixture of carbon vapor, the rare inert gas (helium or argon), and the vapors of catalysts.

The vaporization is the consequence of the energy transfer from the arc to the anode made of graphite doped with catalysts.

Nanotubos de Carbono: Funcionalização

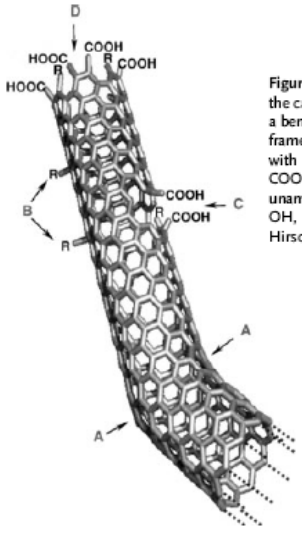

Figure 1. Typical defects in a SWNT. A) Five-or seven-membered rings in the carbon framework, instead of the normal six-membered ring, leads to a bend in the tube. B) sp^3-hybridized defects (R = H and OH). C) Carbon framework damaged by oxidative conditions, which leaves a hole lined with –COOH groups. D) Open end of the SWNT, terminated with –COOH groups. Besides carboxy termini, the existence of which has been unambiguously demonstrated, other terminal groups such as $-NO_2$, –OH, –H, and =O are possible. Reprinted with permission from A. Hirsch, *Angew. Chem. Int. Ed.* 2002, *41*, 1853. Copyright 2002 Wiley-VCH.

Fonte: *Banerjee, S. et al., Adv. Mater. , 2005, 17.*

Nanotubos de Carbono: Funcionalização

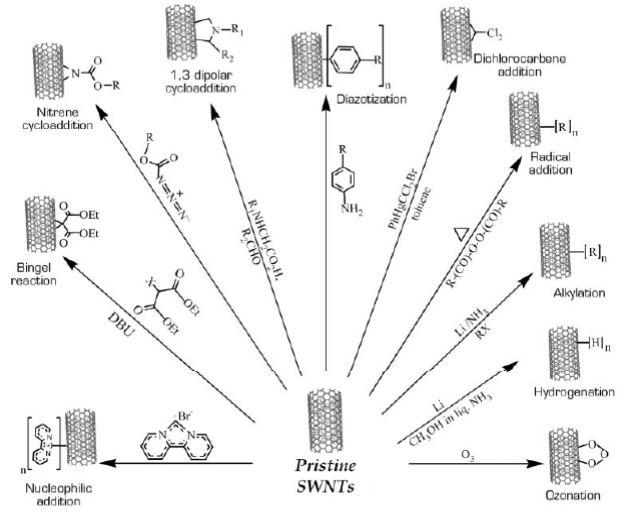

Fonte: *Banerjee, S. et al., Adv. Mater. , 2005, 17.*

Nanotubos de Carbono: Funcionalização

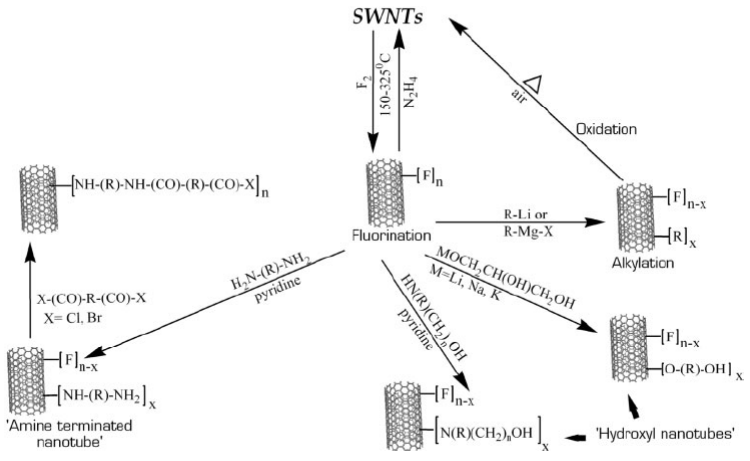

Fonte: *Banerjee, S. et al., Adv. Mater. , 2005, 17.*

Espectroscopia Raman

Quando uma molécula é irradiada, a energia pode ser transmitida, absorvida, ou espalhada. A espectroscopia Raman é baseada na detecção da luz espalhada.

No espalhamento Rayleigh (***elástico***), a interação da molécula com o fóton não provoca mudanças nos níveis de energia vibracional e/ou rotacional da molécula. *Assim **as freqüências da luz incidente e espalhada são as mesmas.***

O efeito Raman pode ser explicado pela colisão ***não-elástica*** entre o fóton incidente e a molécula. Isto muda os níveis das energias vibracional e/ou rotacional da molécula por um incremento ($\pm \Delta E$). Pela lei de conservação de energia, isto significa que as energias dos fótons incidente e espalhado serão diferentes, ou seja $\nu_{incidente} \neq \nu_{espalhada}$. Se a molécula absorve energia, ΔE é positiva, $\nu_{incidente} > \nu_{espalhada}$,, estas são as ***linhas Stokes*** do espectro (regra de Stokes de fluorescência, $\nu_{incidente} > \nu_{fluorescência}$). Se a molécula perde energia, ΔE é negativa, $\nu_{incidente} < \nu_{espalhada}$, *linhas **anti Stokes*** do espectro.

Raman Spectroscopy: Some Sources

General Principles and Instrumentation:

Principles of Instrumental Analysis, by Douglas A. Skoog, F. James Holler, Timothy A. Nieman

Inorganic:

Infrared and Raman Spectra of Inorganic and Coordination Compounds : Theory and Applications in Inorganic Chemistry (Volume A) by Kazuo Nakamoto

Infrared and Raman Spectra of Inorganic and Coordination Compounds : Applications in Coordination, Organometallic, and Bioinorganic Chemistry (Volume B) by Kazuo Nakamoto

Organic:

The Handbook of Infrared and Raman Characteristic Frequencies of Organic Molecules by Daimay Lin-Vien, et al

Raman Spectroscopy: Overview

- A vibrational spectroscopy
  - IR and Raman are the most common vibrational spectroscopies for assessing molecular motion and fingerprinting species
  - Based on **inelastic** scattering of a monochromatic excitation source
  - Routine energy range: 200 - 4000 cm^{-1}
- Complementary selection rules to IR spectroscopy
  - Selection rules dictate which molecular vibrations are probed
  - Some vibrational modes are both IR and Raman active
- Great for many real-world samples
  - Minimal sample preparation (gas, liquid, solid)
  - Compatible with wet samples and normal ambient
  - Achilles Heal is sample fluorescence

Raman Spectroscopy: General

- IR and Raman are both useful for Fingerprinting

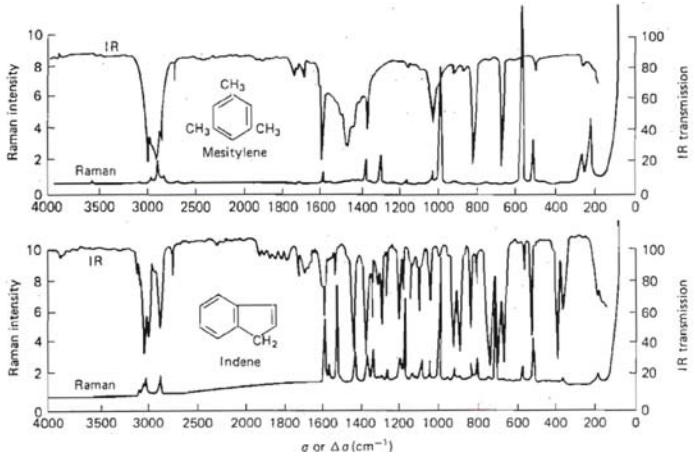

- Symmetry dictates which are active in Raman and IR

Raman Spectroscopy: General

- Group assignments identify characteristic vibrational energy

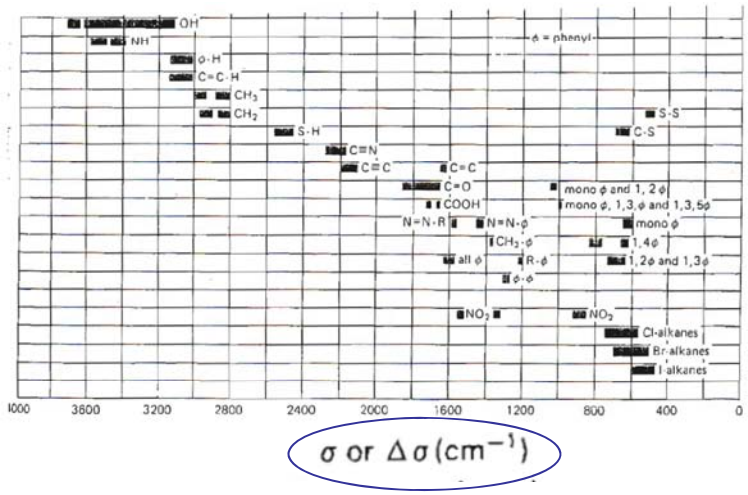

Raman Spectroscopy: Classical Treatment

- Number of peaks related to degrees of freedom

  DoF = 3N - 6 (bent) or 3N - 5 (linear) for N atoms

- Energy related to harmonic oscillator

$$\sigma \text{ or } \Delta\sigma = \frac{c}{2\pi}\sqrt{\frac{k(m_1+m_2)}{m_1 m_2}}$$

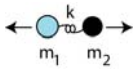

- Selection rules related to symmetry

  Rule of thumb: symmetric=Raman active, asymmetric=IR active

CO_2	H_2O
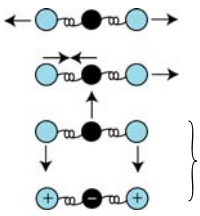 Raman: 1335 cm^{-1} IR: 2349 cm^{-1} IR: 667 cm^{-1}	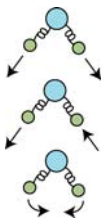 Raman + IR: 3657 cm^{-1} Raman + IR: 3756 cm^{-1} + IR: 1594 cm^{-1}

Main Optical Transitions: Absorption, Scattering, and Fluorescence

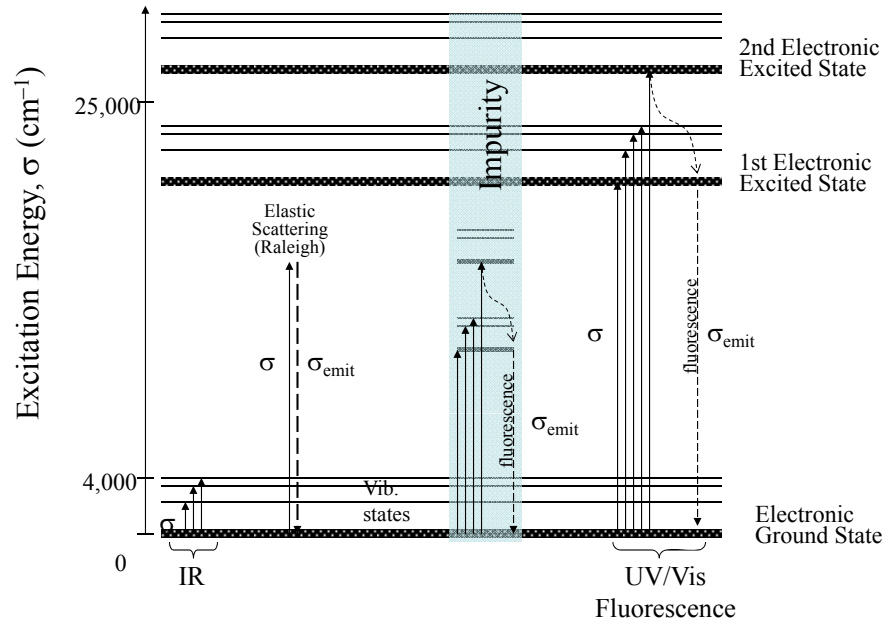

Raman Spectroscopy: Absorption, Scattering, and Fluorescence

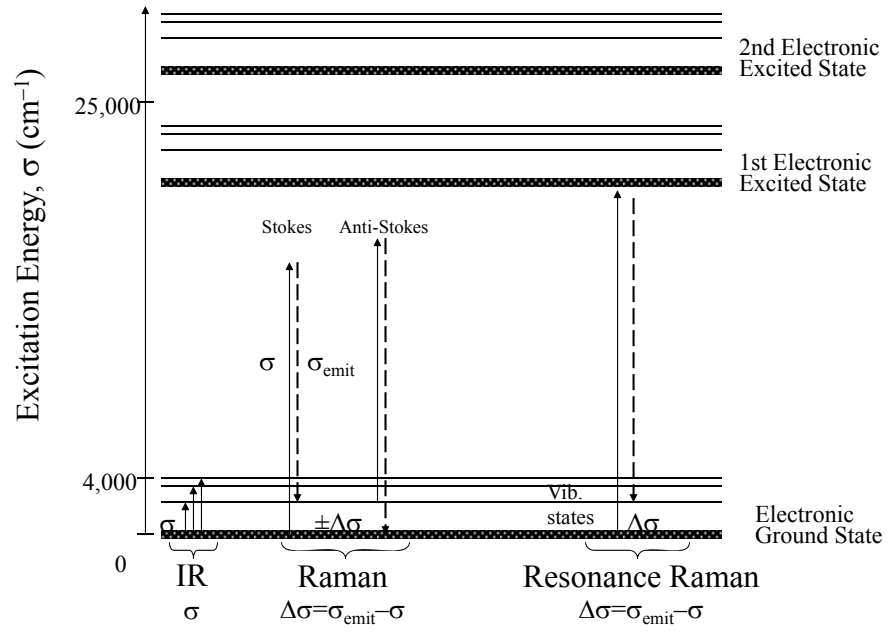

Raman Spectroscopy: At NTUF, you pick the Laser Excitation

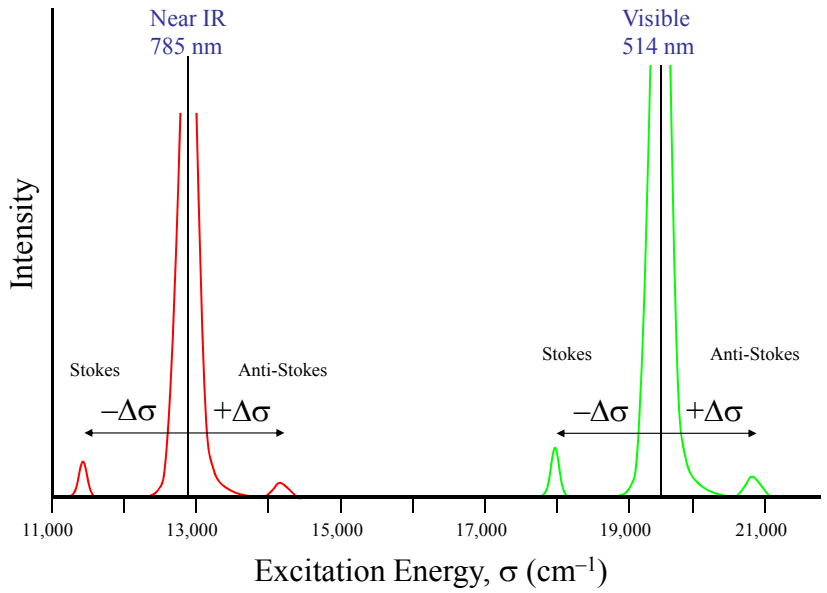

Raman Spectroscopy: Absorption, Scattering, and Fluorescence

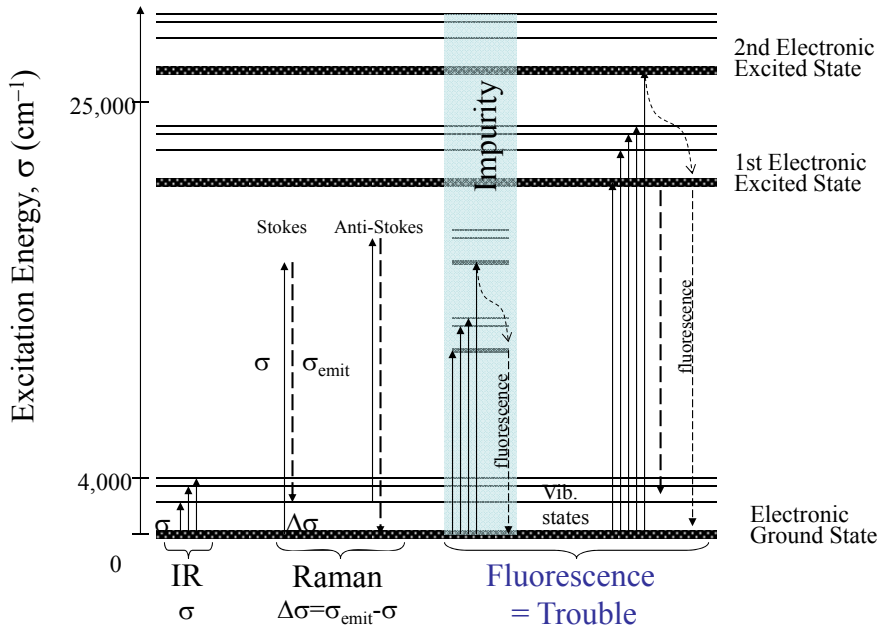

Muito bom !!!

ELSEVIER

Available online at www.sciencedirect.com
SCIENCE DIRECT®

Physics Reports ▮▮▮ (▮▮▮) ▮▮▮–▮▮▮

PHYSICS REPORTS

www.elsevier.com/locate/physrep

Raman spectroscopy of carbon nanotubes

M.S. Dresselhaus[a,*], G. Dresselhaus[b], R. Saito[c], A. Jorio[d]

[a]*Department of Physics and Department of Electrical Engineering and Computer Science, Massachusetts Institute of Technology, Room 13-3005, Cambridge, MA 02139, USA*
[b]*Francis Bitter Magnet Lab, MIT, Cambridge, MA 02139, USA*
[c]*Department of Physics, Tohoku University, and CREST, JST, Sendai 980-8578, Japan*
[d]*Depto. de Fisica, Universidade Federal de Minas Gerais, Belo Horizonte - MG 30123-970, Brazil*

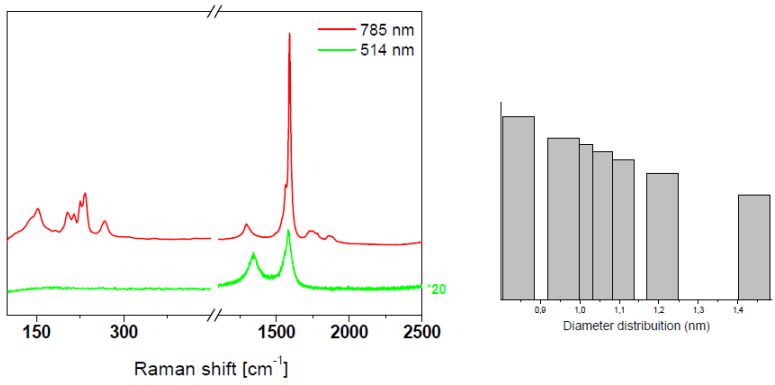

Fig. 1- (a) Different Raman spectra of SWCNT obtained from red laser (785 nm) and green laser (514 nm), (b) and its diameter distribution.

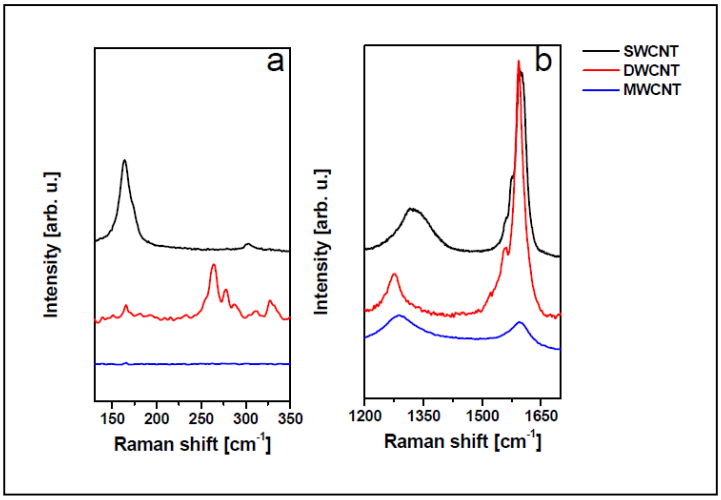

Fig. 3- Different Raman spectra obtained from SWCNT, DWCNT and MWCNT (a) RBM and (b) D and G bands (laser excitation 785 nm)..

The radial breathing mode is a commonly used technique to evaluate the diameter of carbon nanotubes. In nanotechnology, a Raman microscope can be used to analyze nanowires to better understand the composition of the structures.

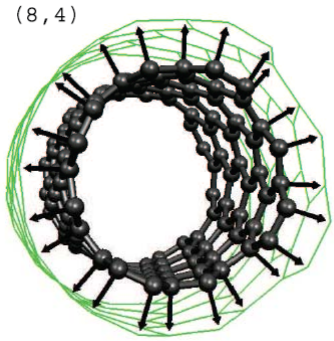

Radial breathing mode of an (8,4) nanotube. The arrows show the phonon eigenvector. The RBM leads to a periodic increase and decrease of the tube diameter as shown by the wire model of the tube.

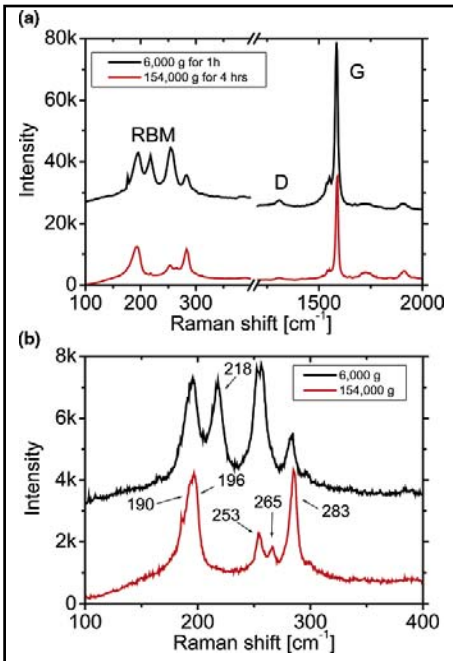

(a) Raman spectrum of a HiPco SWNTs suspension after centrifugation at 6.000 g for 1 h and after centrifugation at 154 000 g for 4 h. (b) RBM frequency region.

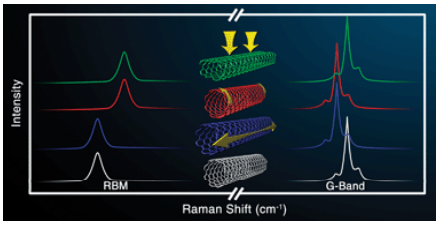

J. Phys. Chem. B, Vol. 109, No. 21, 2005

Grafeno

- Graphene is an allotrope of carbon. In this material, carbon atoms are arranged in a regular hexagonal pattern. Graphene can be described as a one-atom thick layer of the mineral graphite, (many layers of graphene stacked together effectively form crystalline flake graphite). Amongst its other well-publicised superlative properties, it is very light, with a 1-square-meter sheet weighing only 0.77 milligrams.
- The Nobel Prize in Physics for 2010 was awarded to Andre Geim and Konstantin Novoselov at the University of Manchester "for groundbreaking experiments regarding the two-dimensional material graphene". In 2013, graphene researchers led by Prof. Jari Kinaret from Sweden's Chalmers University of Technology, secured a €1 billion grant from the European Union to be used for further research into development of potential applications of graphene

Brief history of graphene

The term graphene first appeared in 1987 to describe single sheets of graphite as one of the constituents of graphite intercalation compounds (GICs). Larger graphene molecules or sheets (so that they can be considered as true isolated 2D crystals) cannot be grown even in principle. In the 1930s, Landau and Peierls (and Mermin, later) showed thermodynamics prevented 2-d crystals in free state, an article in Physics Today reads:

"Fundamental forces place seemingly insurmountable barriers in the way of creating [2D crystals] ... Nascent 2D crystallites try to minimize their surface energy and inevitably morph into one of the rich variety of stable 3D structures that occur in soot. But there is a way around the problem. Interactions with 3D structures stabilize 2D crystals during growth. So one can make 2D crystals sandwiched between or placed on top of the atomic planes of a bulk crystal. In that respect, graphene already exists within graphite ... One can then hope to fool Nature and extract single-atom-thick crystallites at a low enough temperature that they remain in the quenched state prescribed by the original higher-temperature 3D growth."

In **2004**: Andre Geim and Kostya Novoselov at Manchester University managed to extract single-atom-thick crystallites (graphene) from bulk graphite: Pulled out graphene layers from graphite and transferred them onto thin silicon dioxide on a silicon wafer in a process sometimes called micromechanical cleavage or, simply, the Scotch tape technique. Since 2004, an explosion in the investigation of graphene in term of synthesis, characterization, properties as well as specifical potential application were reported.

Introduction to graphene

Graphene *is a one-atom-thick planar sheet of* sp^2*-bonded carbon atoms that are densely packed in a honeycomb crystal lattice*

The name 'graphene' comes from graphite + -ene = graphene

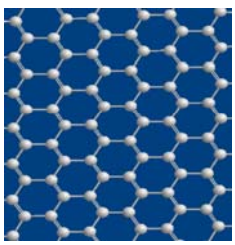

Molecular structure of graphene

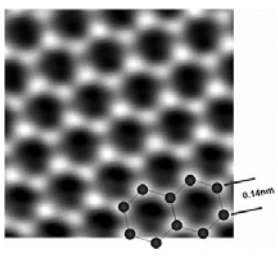

High resolution transmission electron microscope images (TEM) of graphene

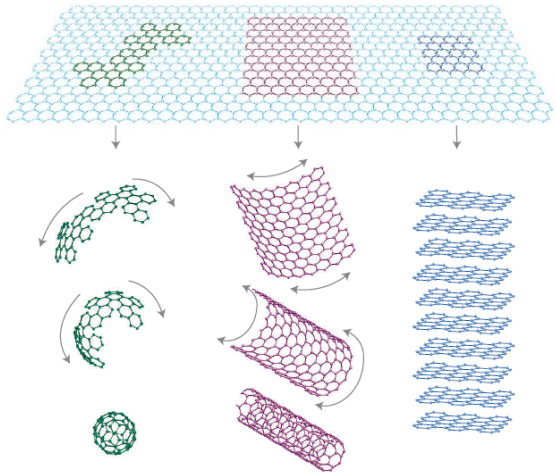

Figure 1 Mother of all graphitic forms. Graphene is a 2D building material for carbon materials of all other dimensionalities. It can be wrapped up into 0D buckyballs, rolled into 1D nanotubes or stacked into 3D graphite.

A. K. Geim & K. S. Novoselov. The rise of graphene. *Nature Materials Vol . 6* ,183-191 (2007).

Properties of graphene

- Electronic properties
- Thermal properties
- Mechanical properties
- Optical properties
- Relativistic charge carriers
- Anomalous quantum Hall effect

Electronic properties

- High electron mobility (at room temperature ~ 200.000 $cm^2/(V \cdot s)$,, ex. Si at RT~ 1400 $cm^2/(V \cdot s)$, carbon nanotube: ~ 100.000 $cm^2/(V \cdot s)$, organic semiconductors (polymer, oligomer): <10 $cm^2/(V \cdot s)$

$$v_d = \mu E$$

Where υ_d is the drift velocity in m/s (SI units)
E is the applied electric field in V/m (SI)
μ is the mobility in $m^2/(V \cdot s)$, in SI units.

- Resistivity of the graphene sheet ~10^{-6} Ω·cm, less than the resistivity of silver (Ag), the lowest resistivity substance known at room temperature (electrical resistivity is also as the inverse of the conductivity σ (*sigma*), of the material, or

$$\rho = \frac{1}{\sigma}$$

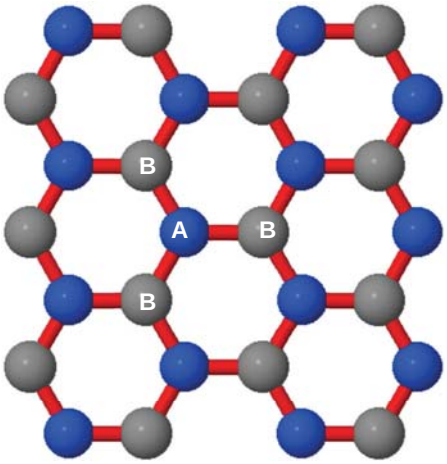

Triangular sublattices of graphene. Each atom in one sublattice (A) has 3 nearest neighbors in sublattice (B) and viceversa.

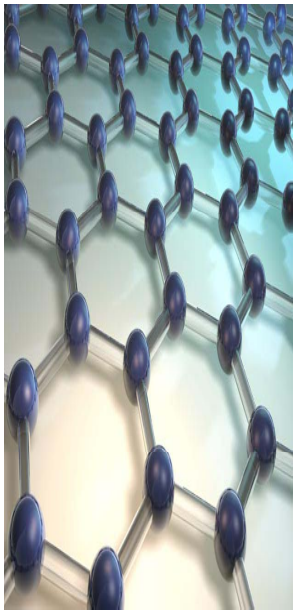

Properties

- **Electronic**
- **Optical**
- **Excitonic**
- **Thermal**
- **Mechanical**
- **Spin transport**
- **Anomalous quantum Hall effect**

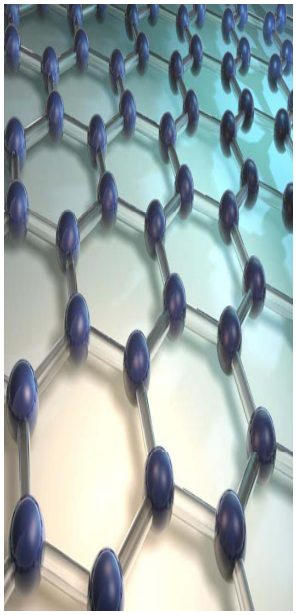

Electronic

• Intrinsic graphene is a semi-metal or zero-gap semiconductor
• remarkably high electron mobility at room temperature, with reported values in excess of 15,000 $cm^2 \cdot V^{-1} \cdot s^{-1}$.
• Fermi velocity $v_F \sim 10^6$ m/s
• resistivity of the graphene sheet would be10^{-6} Ω·cm. This is less than the resistivity of silver, the **lowest resistivity substance known at room temperature!**

Electronic

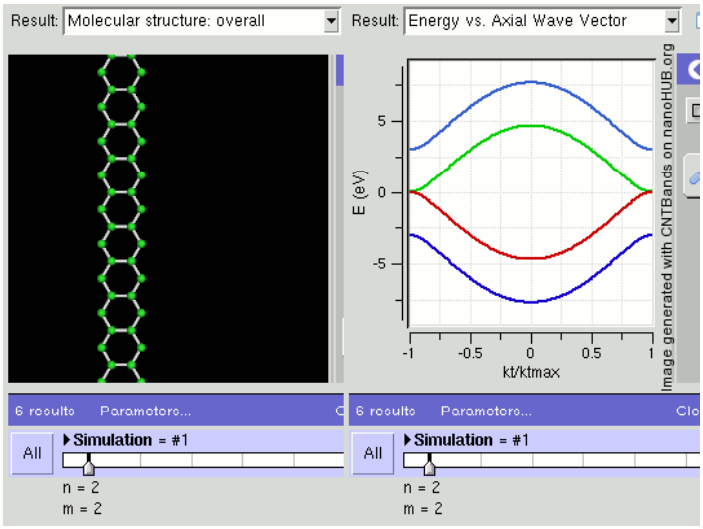

GNR band structure for zig-zag orientation. Tightbinding calculations show that zigzag orientation is always metallic.

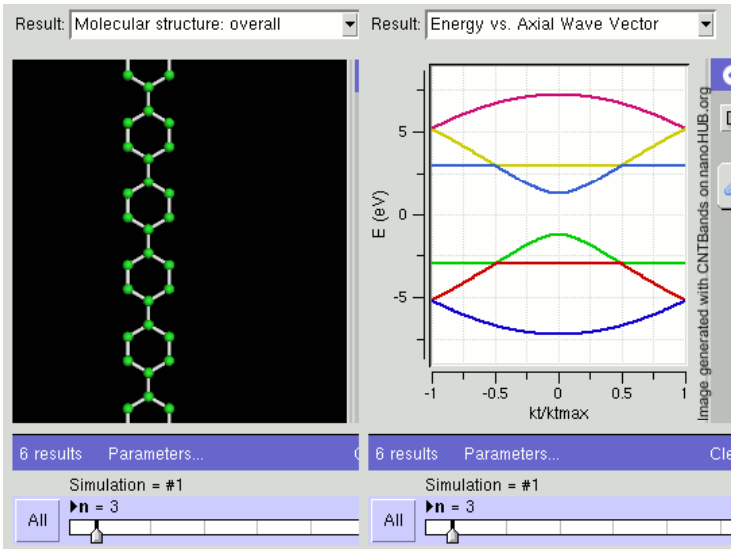

GNR band structure for arm-chair orientation. Tightbinding calculations show that armchair orientation can be semiconducting or metallic depending on width (chirality).

a) Raman spectra of 7 layered GO thin films recorded with λ = 633nm laser with a lateral beam dimension of 2 mm. Spectra of pristine GO (black curve), reduced GO via exposure to hydrazine monohydrate vapor at 80 8C followed by annealing at 200 8C (red curve) and GO reduced by annealing only at 1100 8C (yellow curve) are shown. In the inset, the I(D)/I(G) ratio and the related average sp2 cluster sizes of GO thin films before and after reduction reported in the literature along with our results are shown. b) TEM image of few layered chemically reduced reduced GO (Scale bar 200 nm). Corresponding diffraction patterns are taken from c) pristine GO and d) chemically reduced GO followed by annealing. Both diffraction patterns show the six-fold rotational symmetry expected for diffraction with the beam incident along the [001] direction. The innermost diffraction spots are from (100) planes (d-spacing 0.21 nm) while the outer are from (110) planes (d-spacing 0.12 nm).

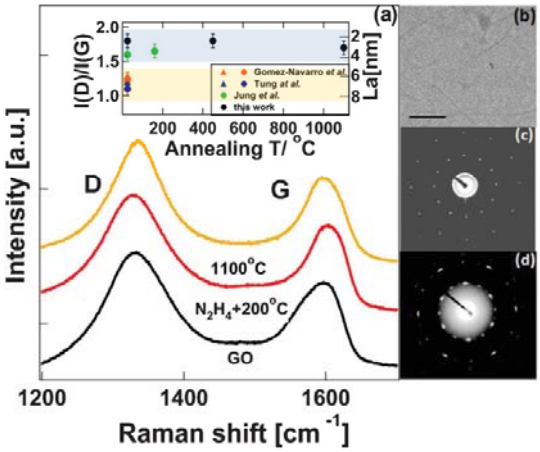

Adv. Funct. Mater. 2009, 19, 2577–2583

Material	Electrical Conductivity (S·m^{-1})	Notes
Graphene	~ 10^8	
Silver	63.0 × 10^6	Best electrical conductor of any known metal
Copper	59.6 × 10^6	Commonly used in electrical wire applications due to very good conductivity and price compared to silver.
Annealed Copper	58.0 × 10^6	Referred to as 100% IACS or International Annealed Copper Standard. The unit for expressing the conductivity of nonmagnetic materials by testing using the eddy-current method. Generally used for temper and alloy verification of aluminium.
Gold	45.2 × 10^6	Gold is commonly used in electrical contacts because it does not easily corrode.
Aluminium	37.8 × 10^6	Commonly used for high voltage electricity distribution cables[citation needed]
Sea water	4.8	Corresponds to an average salinity of 35 g/kg at 20 °C.[1]
Drinking water	0.0005 to 0.05	This value range is typical of high quality drinking water and not an indicator of water quality
Deionized water	5.5 × 10^{-6}	Conductivity is lowest with monoatomic gases present; changes to 1.2 × 10^{-4} upon complete de-gassing, or to 7.5 × 10^{-5} upon equilibration to the atmosphere due to dissolved CO_2.[2]
Jet A-1 Kerosene	50 to 450 × 10^{-12}	[3]
n-hexane	100 × 10^{-12}	
Air	0.3 to 0.8 × 10^{-14}	

Properties of graphene

Mechanical properties

- High Young's modulus (~1,100 Gpa) High fracture strength (125 Gpa)

- Graphene is as the strongest material ever measured, some 200 times stronger than structural steel

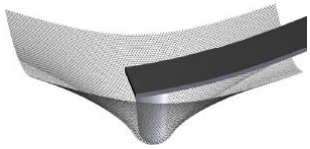

A representation of a diamond tip with a two nanometer radius indenting into a single atomic sheet of graphene *(Science,* **321** (5887): 385)

Optical properties

- Monolayer graphene absorbs $\pi\alpha \approx 2.3\%$ of white light (97.7 % transmittance), where α is the fine-structure constant.

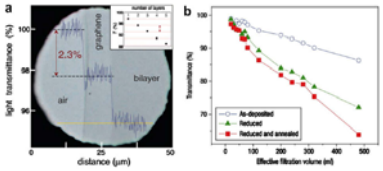

Preparation and characterization graphene

Preparation methods

Top-down approach (From graphite)

- Micromechanical exfoliation of graphite (Scotch tape or peel-off method)
- Creation of colloidal suspensions from graphite oxide or graphite intercalation compounds (GICs)

Bottom up approach (from carbon precursors)

- By chemical vapour deposition (CVD) of hydrocarbon
- By epitaxial growth on electrically insulating surfaces such as SiC
- Total Organic Synthesis

Table 1 – Advantages and disadvantages for techniques currently used to produce graphene.

	Advantages	Disadvantages
Mechanical exfoliation	Low cost and easy No special equipment needed, SiO_2 thickness is tuned for better contrast	Serendipitous Uneven films Labor intensive (not suitable for large-scale production)
Epitaxial growth	Most even films (of any method) Large scale area	Difficult control of morphology and adsorption energy High-temperature process
Graphene oxide	Straightforward up-scaling Versatile handling of the suspension Rapid process	Fragile stability of the colloidal dispersion Reduction to graphene is only partial

Ref: Carbon, 48, 2127–2150 (2010)

Characterization methods

Scanning Probe Microscopy (SPM): | Raman Spectroscopy | Transmission electron Microscopy (TEM) | X-ray diffraction (XRD)

- Atomic force microscopes (AFMs)
- Scanning tunneling microscopy (STM)

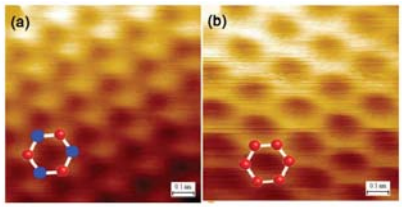

Figure 7. (a) STM image of graphite showing only the three carbons that eclipse a neighbor in the sheet directly below. (b) In contrast, all six carbons are equivalent and thus visible in mechanically exfoliated single-layer graphene. (Reprinted with permission from ref 79. Copyright 2007 PNAS.)

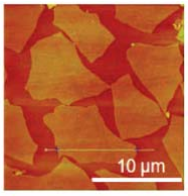

Atomic force microscopy images of a graphite oxide film deposited by Langmuir-Blodgett assembly

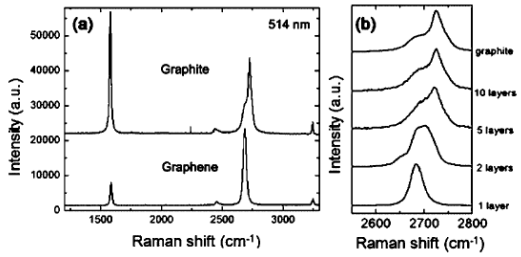

Raman Spectroscopy

Figure 8. Raman spectroscopy is a powerful diagnostic tool for the study of graphene. Both the G (near 1584 cm^{-1}) and G′ (near 2700 cm^{-1}) bands undergo significant changes due to the thickness of AB stacked flakes, as produced by mechanical exfoliation. (Reprinted with permission from ref 80. Copyright 2006 American Physical Society.)

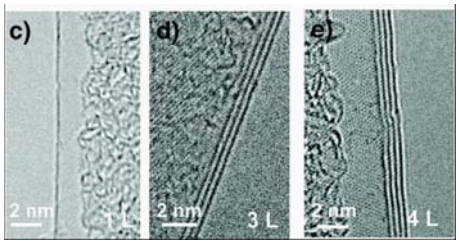

TEM images show the nucleation of (c) one, (d) three, or (e) four layers during the growth process

Transmission electron Microscopy (TEM)

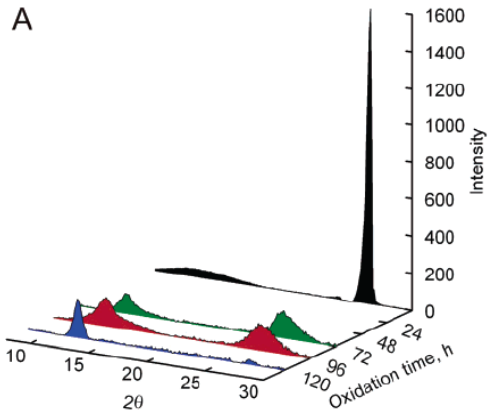

X-ray diffraction (XRD)

XRD patterns of 400 *um diameter graphite flakes oxidized for various lengths of time.*

Preparation methods and discussions

Top-down approach
(From graphite)

Direct exfoliation of graphite

Graphite intercalation compound

Graphite oxide method

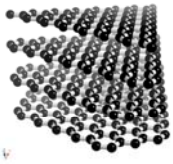

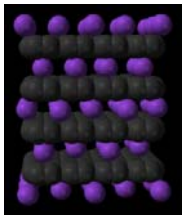

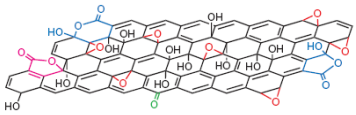

Nature nanotechnology ,vol 4, APRIL (2009)

Table 1 | Comparison of a set of chemical approaches to produce colloidal suspensions of CMG sheets

Ref.	Starting materials	Dispersible solvents	Concentration (mg ml^{-1})	Lateral size	Thickness (nm)
34	GO/MH	Water	1	—	—
36	GO/MH	Water	0.5	Several hundred nm	~1
39	GO/MH	Water	0.1	—	~1.7
40	GO/MH	Water	7	Several hundred nm	~1
42	GO/H	Water/methanol, acetone, acetonitrile mixed solvents	3–4	Several hundred nm	~1.2
45	GO/MH	DMF, NMP, DMSO, HMPA	1	~560 nm	~1
46	GO/H	Water, acetone, ethanol, 1-propanol, ethylene glycol, DMSO, DMF, NMP, pyridine, THF	0.5	100–1,000 nm	1.0–1.4
49	GO/O	DMF, THF, CCl_4, DCE	0.5	—	0.5–2.5
50	Graphite fluoride	DCB, MC, THF	0.002–0.54	1,600 nm	~0.95
51	GO/S	DMF, DMAc, NMP	1	Several hundred nm	1.8–2.2
52	GO/MH	Hydrazine	1.5	Up to 20 μm × 40 μm	~0.6
54	GO/S	THF	<0.48	—	1–2
55, 56, 10	GO/S	NMP, DMF, DCB, THF, nitromethane	0.1	100–2,500 nm	1.1–3.5 (ave. 1.75)
57	GO/H	Ethanol	1	Several hundred nm	~2
59	Graphite powder	NMP, DMAc, GBL, DMEU	0.01	Several μm	1–5
60	GIC	NMP	0.15	Several hundred nm	~0.35
61	EG	DCE	0.0005	Nanoribbon (width <10 nm)	1–1.8
62	EG	DMF	—	~250 nm	~1
63	EG	Water, DMF, DMSO	0.015–0.020	Several hundred nm to a few μm	2–3 (2–3 layers of graphene)
64	Graphite rod	DMF, DMSO, NMP	1	500–700 nm	~1.1

GO, graphite oxide; MH, modified Hummers method; H, Hummers method; O, their own method; S, Staudenmaier method; EG, expandable graphite; GIC, graphite intercalation compound; DMF, dimethylformamide; DMAc, *N,N*′-dimethylacetamide; DMSO, dimethylsulphoxide; NMP, *N*-methylpyrrolidone; THF, tetrahydrofuran; MC, dichloromethane; DCE, 1,2-dichloroethane; DCB, 1,2-dichlorobenzene; HMPA, hexamethylphosphoramide; GBL, γ-butyrolactone; DMEU, 1,3-dimethyl-2-imidazolidinone.

Direct exfoliation of graphite

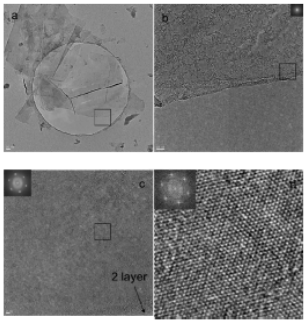

Figure 1. TEM images of single layer graphene from HOPG dispersion showing (a) monolayer and few layer of graphene stacked with smaller flakes; (b) selected edge region from (a); (c) selected area from (b) with FFT inset; (d) HRTEM of boxed region in (c) showing lattice fringes with FFT inset.

NANO LETTERS
XXXX
Vol. xx, No. x

High-Yield Organic Dispersions of Unfunctionalized Graphene

Christopher E. Hamilton, Jay R. Lomeda, Zhengzong Sun, James M. Tour,* and Andrew R. Barron*

Richard E. Smalley Institute for Nanoscale Science and Technology and Department of Chemistry, Rice University, Houston, Texas 77005

Received May 26, 2009; Revised Manuscript Received July 13, 2009

We demonstrate herein a simple, high-yield method of producing homogeneous dispersions of graphene nanosheets in ortho-dichlorobenzene (ODCB) from various graphite materials. The advantage of our method lies in its high yield, its simplicity, and its avoidance of harsh oxidation chemistry.

Dispersions of microcrystalline synthetic graphite have a concentration of 0.03 mg mL-1. Dispersions of expanded graphite and HOPG are less concentrated (0.02 mg mL-1).

Direct exfoliation of graphite

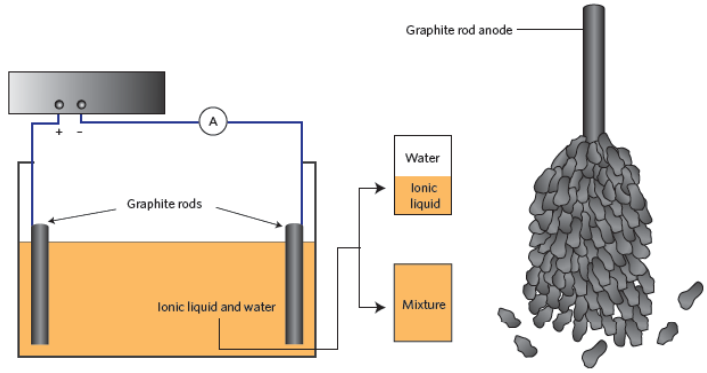

Graphene sheets ionic-liquid-modified by electrochemistry using graphite electrodes.

Liu, N. *et al. One-step ionic-liquid-assisted electrochemical synthesis of ionicliquid-*functionalized graphene sheets directly from graphite. *Adv. Funct. Mater.* **18, 1518–1525 (2008).**

From graphite intercalation compound

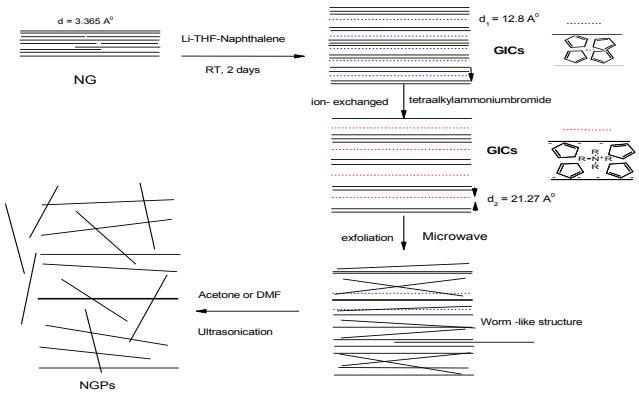

Quang Trung Truong and Dai Soo Lee, IC-ME&D 2010, Sunchon, Korea (*Manuscript for Journal of nanosciences and nanotechnology*)

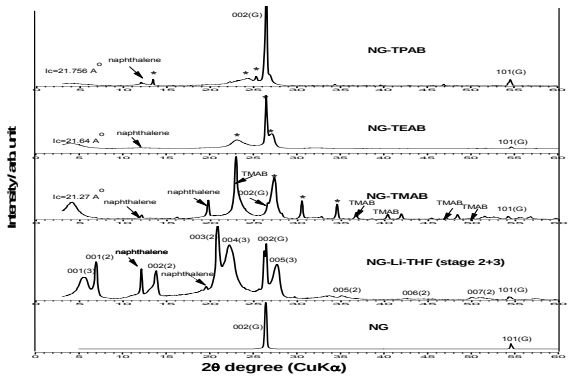

Fig. 1. XRD patterns of NG, ternary NG-Li-THF and GICs of NG with TAAB: tetramethyl (NG-TMAB), tetraethyl-(NG-TEAB) and tetrapropyl- (NG-TPAB). G denoted graphite phase (002) and asterisk * denoted unidentified phases.

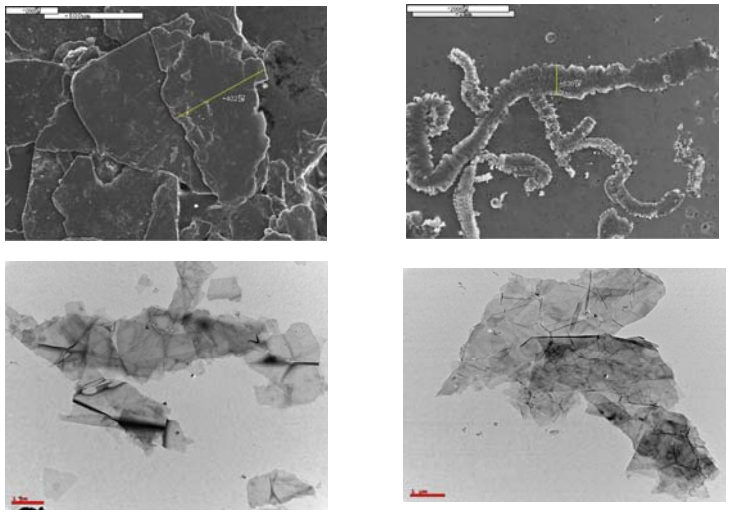

Graphite intercalation compound

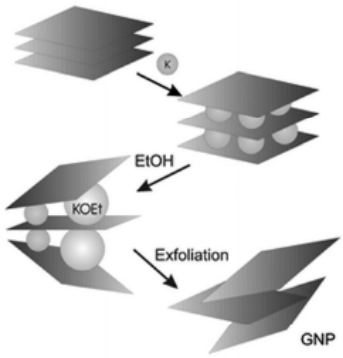

Figure 2. Schematic diagram showing the intercalation and exfoliation process to produce thin slabs of graphite. Potassium is inserted between the layers and reacted violently with alcohols. The exfoliated slabs are ~30 layers thick. (Reprinted with permission by The Royal Society of Chemistry from ref 60.)

J. Mater. Chem. ***2005, 15, 974.***

Graphite oxide method (Most common and high yield method)

Graphite

Oxidation (Hummers'method)

H_2SO_4/ $KMnO_4$
H_2SO_4/$KClO_3$
Or $H2SO_4$/HNO_3
……

Graphite Oxide

H_2O

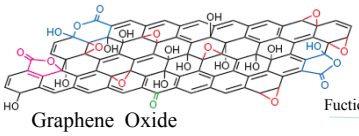

Graphene Oxide
monolayer or few layers

Ultrasonication (exfoliation

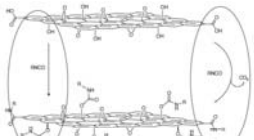

Fuctionalization (for better dispersion)

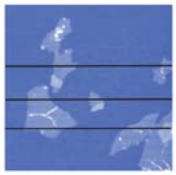

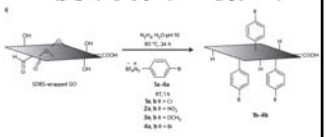

Chemical reduction to restore graphitic structures

Making composite with polymers

Graphite oxide method

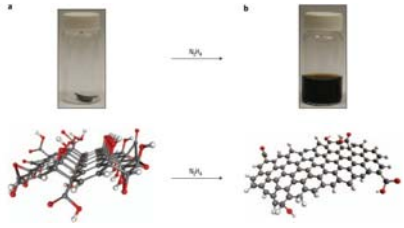

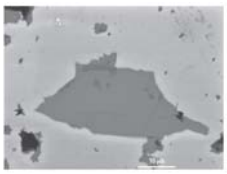

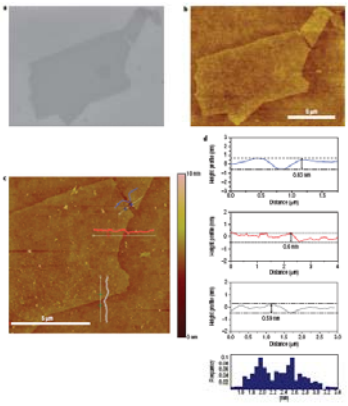

Tung, V. C., Allen, M. J., Yang, Y. & Kaner, R. B. High-throughput solution processing of large-scale graphene. *Nature Nanotech.* ***4, 25–29 (2008).***

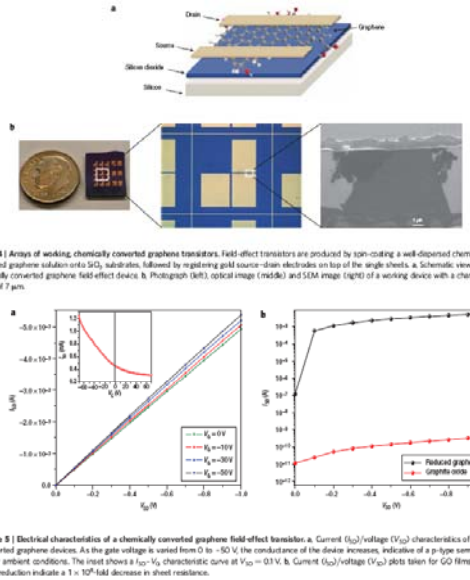

Figure 4 | Arrays of working, chemically converted graphene transistors. Field-effect transistors are produced by spin-coating a well-dispersed chemically converted graphene solution onto SiO_2 substrates, followed by registering gold source–drain electrodes on top of the single sheets. a, Schematic view of a chemically converted graphene field-effect device. b, Photograph (left), optical image (middle) and SEM image (right) of a working device with a channel length of 7 μm.

Figure 5 | Electrical characteristics of a chemically converted graphene field-effect transistor. a, Current (I_{SD})/voltage (V_{SD}) characteristics of chemically converted graphene devices. As the gate voltage is varied from 0 to −50 V, the conductance of the device increases, indicative of a p-type semiconductor under ambient conditions. The inset shows a I_{SD}–V_G characteristic curve at V_{SD} = −0.1 V. b, Current (I_{SD})/voltage (V_{SD}) plots taken for GO films before and after reduction indicate a 1 × 10^6-fold decrease in sheet resistance.

Graphite oxide method

More intercalation for better exfoliation to monolayers

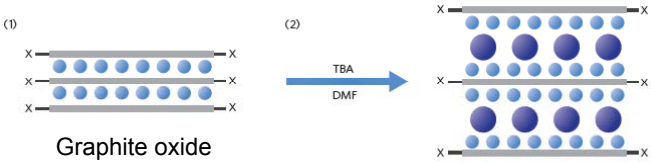

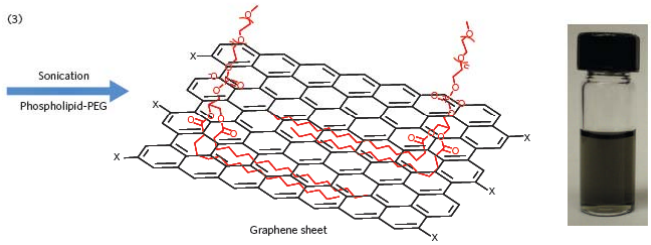

Bottom up approach
(from carbon precursors)

Table 2 – Synoptic table of the graphene growth methods on both metals and carbides substrates. Acronyms are as follows: L, single layer coverage; ML, monolayer; T, temperature; STM, scanning tunneling microscopy; LEED, low-energy electron diffraction; AES, Auger electron spectroscopy; AFM, atomic force microscopy; PCM, point-contact microscopy; XPS, X-ray photoemission spectroscopy; ARUPS, angle-resolved ultraviolet photo-electron spectroscopy; SEELFS, surface extended-energy-loss fine-structure; SEM, scanning electron microscopy; XPD, X-ray photoelectron diffraction; TDS, time-domain spectroscopy; LEIS, low-energy ion spectroscopy.

Substrate		Growth condition (gas, T, exposure)	Experimental technique	Edges	Comment (a_C = 0.245 nm)	Ref.
Metals	Pt(111)	Benzene (C_6H_6), T = 1000 K. 1–5L: non-graphitic film; >5L: full coverage	STM, LEED, AES	Hexagonal arrangement beyond edges		[83]
		Ethylene (C_2H_4), T = 800 K. 5L exposure (If T > 1000 K: graphitic island)	LEED, STM	No clear hexagonal arrangement; No growth over the edges	a_{Pt}=0.278 nm $a_{Moiré'}$=2.2 nm	[55]
		HOPG on 1ML graphitic film	AFM, PCM	Continuous film from upper terrace to lower terrace	0.738 nm < a < 2.1 nm	[239]
	Pt(755)	Chemical vapor deposition	LEED, XPS, ARUPS	Formation of large sheet		[240]
	Ni(111)	Chemical vapor deposition	LEED, AES vibrational spectro		Evidence of Fuchs–Kliewer phonons	[87]
	Ni(110)	Carbon monoxide (CO), T = 600 K. 90000L exposure	SEELFS		Graphitic layer on [110] faces	[241]
	Ru(001)	Ethylene (C_2H_4), T = 1270 K. T-dependent solubility gradient	LEEM, SEM, μ-Raman, AES, electrical	No growth "uphill" over the edges	a_{Ru} = 0.271 nm a = 0.145 nm (1st layer) $a_{Moiré'}$ = 3 nm	[56]
	Ir(111)	Ethylene (C_2H_4), T > 1100 K. 1L exposure	STM	Growth beyond both side of the edges	a_{Ir} = 0.272 nm $a_{Moiré'}$ = 2.5 nm	[86]
	Co(0001)	Acetylene (C_2H_2), T = 410 K. 0.6L-3.6L exposure	XPS, XPD, LEED, TDS, LEIS		K enhances the coverage of the surface	[242]
Carbides	nH–SiC (n = 1,2,...)	Si sublimation, T ~ 1670 K.	LEED, X-ray, STM	Formation of large continuous sheet over terraces		[69]
	TiC(111)	Chemical Vapor Deposition on faceted surface, T = 1770 K	XPS, ARUPS, LEED	No edge-localized state	Growth on each facet	[78]
	TiC(410)	Chemical Vapor Deposition on platelets surface, T = 1770 K	XPS, ARUPS, LEED	No growth over the edges	Nanoribbon growth (~.1–2 nm)	[78]
	TaC(111)	Ethylene (C_2H_4), T = 1570 K 10000L exposure, T = 1270 K	AES, LEED, STM	Coverage is interrupted at terrace interface	a = 0.249 nm (1st layer) a = 0.247 nm (2nd layer)	[80]

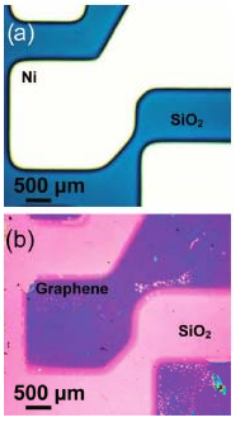

Fig. 5 – Nickel-grown graphene. (a) Optical image of a pre-patterned Ni film on SiO_2/Si. CVD graphene is grown on the surface of the Ni pattern. (b) Optical image of the grown graphene transferred intact from the Ni surface in (a) to another SiO_2/Si substrate. Reproduced with permission from Ref. [58]. Copyright 2009 American Chemical Society.

Total Organic Synthesis

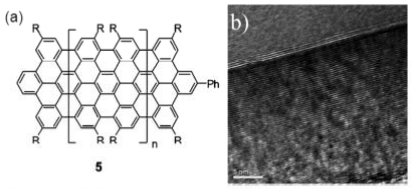

Figure 17. Polyacyclic aromatic hydrocarbons (PAHs) may offer a ground-up synthesis of graphene. (a) Chemical structure of PAHs and (b) TEM of a nanoribbon synthesized by Mullen. (Reprinted with permission from ref 35. Copyright 2008 American Chemical Society.)

Yang, X. Y.; Dou, X.; Rouhanipour, A.; Zhi, L. J.; Rader, H. J.; Mullen, K. *J. Am. Chem. Soc.* ***2008, 130, 4216.***

Graphene nanoribbons (from carbon nanotube)

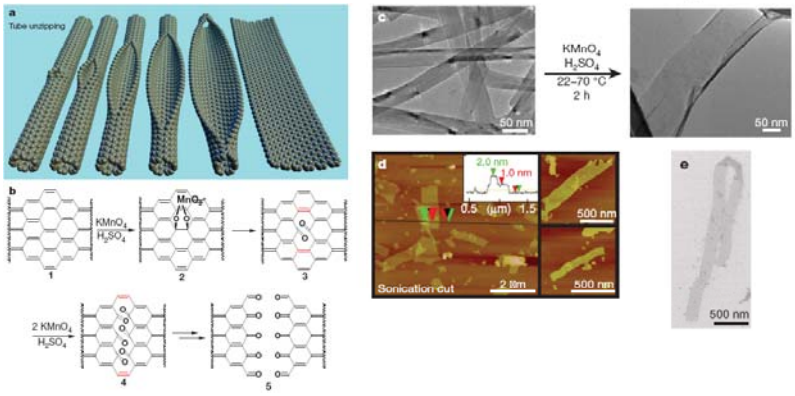

NATURE, Vol , 458, 16 , April (2009)

Potential application of graphene

- **Single molecule gas detection**
- **Graphene transistors**
- **Integrated circuits**
- **Transparent conducting electrodes for the replacement of ITO**
- **Ultracapacitors**
- **Graphene biodevices**
- **Reinforcement for polymer nanocomposites: Electrical, thermally conductive nanocomposites, antistatic coating, transparent conductive composites..ect**

Electrical, thermally conductive nanocomposites

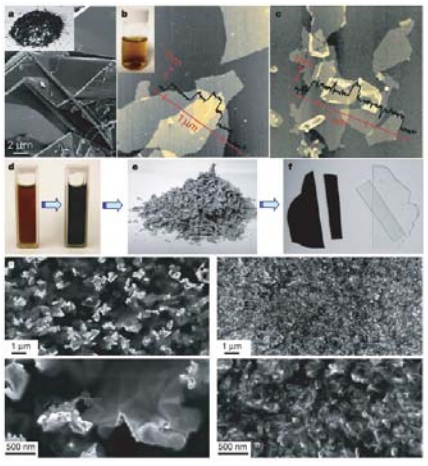

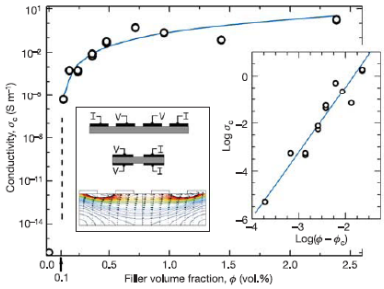

Figure 3 | Electrical conductivity of the polystyrene–graphene composites as a function of filler volume fraction. Main figure, composite conductivity, σ_c, plotted against filler volume fraction, ϕ. Right inset, logσ_c plotted against log($\phi - \phi_c$), where ϕ_c is the percolation threshold (see text). Solid lines in both graphs are calculated conductivities based on the fitting (inset, log–log plot) of the experimental data to the effective conductivity equation described in the text. Fitted parameters are: $t = 2.74 \pm 0.20$, $\sigma_f = 10^{4.92 \pm 0.52}$ S m^{-1} and $\phi_c = 0.1$ vol.%. Left inset: top and middle diagrams show the four-probe setup for in-plane and transverse measurements, respectively; bottom diagram, one of the computed distributions of the current density (contour lines) with local directions and magnitude (shown by arrows) in a specimen for the following conditions—the sample thickness is twice the electrode width and the gap between them, and the in-plane resistivity is 10 times lower than the transverse resistivity.

Nature, Vol. 442, 20,July (2006)

small

Graphene nanosheets

Oriented Arrays of Graphene in a Polymer Matrix by in situ Reduction of Graphite Oxide Nanosheets**

*Seema Ansari, Antonios Kelarakis, Luis Estevez, and Emmanuel P. Giannelis**

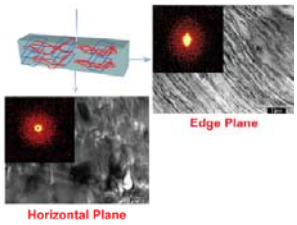

Figure 1. Schematic representation of the GO–Nafion morphology, showing both platelike GO nanosheets (rectangular shape) and bundle of elongated aggregates of ionic domains aligned parallel to the film surface. TEM images and 2D SAXS profiles show the horizontal and th edge plane, respectively.

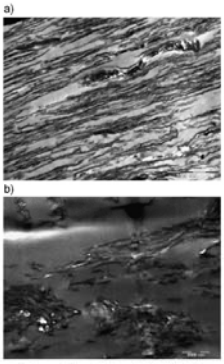

Figure 2. TEM image of the edge plane of a) GS–Nafion 2-step nanocomposite and b) GS–Nafion 1-step nanocomposite.

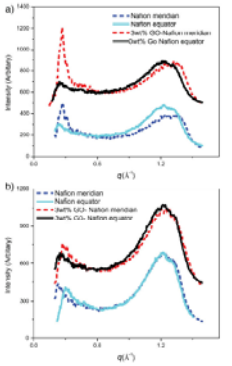

Figure 3. Meridian and equatorial WAXD patterns from a) transverse and b) normal planes for pure Nafion and 3 wt% GO–Nafion films. (For clarity the curves are displaced along the y axis.)

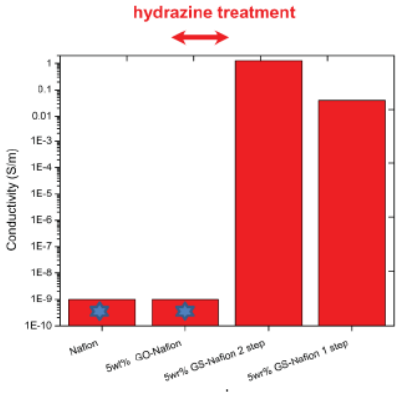

Figure 5. Conductivity of neat Nafion and Nafion nanocomposites at RH < 1ppm. The stars indicate that conductivity values fall below the detection limit of the apparatus used (1×10^{-9} S m^{-1}).

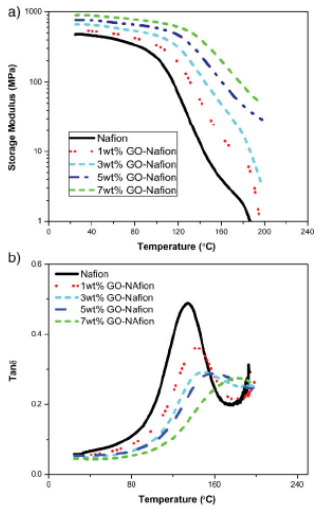

Figure 4. a) Storage modulus and b) tan δ of Nafion and GO–Nafion nanocomposites as a function of temperature.

Transparent conducting electrodes

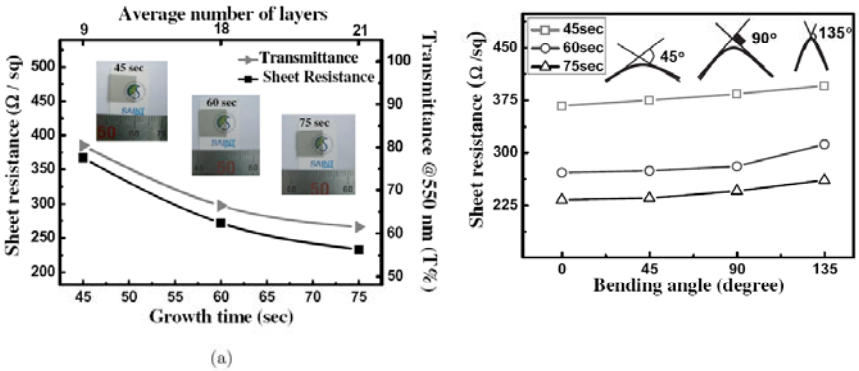

(a)

Table 1. Comparison of our results with other transparent conducting film properties of sheet resistance, transmittance, and thickness.

Transparent conducting film by	Sheet resistance (Ω/sq)	Transmittance (T%)	Thickness (nm)	References
CVD graphene	367	80	~3	
	272	66	~6	
	233	62	~7	
HOPG (monolayer)	29.4	97.7	0.34	Nair[19]
Reduced	1800	65	10–11	Wang[13]
graphite-oxide	1900	90	8.1	Becerril[20]
Carbon nanotube	50	~68	40	Contreras[21]
	30	~75	50	Wu[22]
	40–70	70–80	40–60	Geng[23]
	200	85	30	Rowell[24]

Reinforcement for polymer nanocomposites

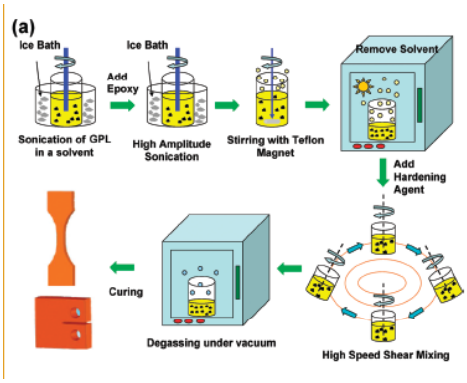

ACS Nano, 2009, 3 (12), pp 3884–3890

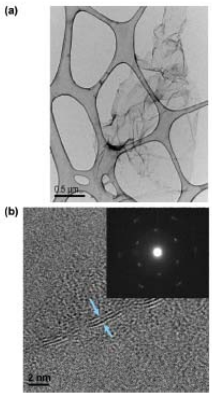

Figure 1. (a) TEM image of a GPL flake deposited on a standard TEM grid, and (b) HRTEM image of the edges of a GPL flake indicating the layered graphene platelet structure. The inset shows the measured electron diffraction pattern.

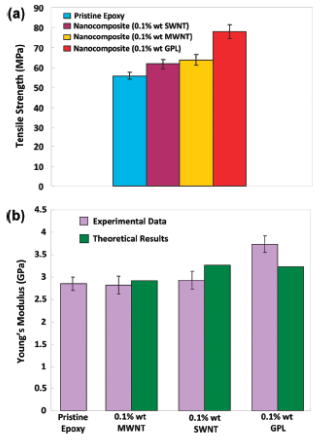

Figure 3. Uniaxial tensile testing. (a) Ultimate tensile strength for the baseline epoxy and GPL/epoxy, MWNT/epoxy, and SWNT/epoxy nanocomposites. The weight fraction of nanofillers for all of the nanocomposite samples tested was fixed at ~0.1%. (b) Young's modulus of nanocomposite samples with ~0.1% weight of GPL, ~0.1% weight of SWNT, and ~0.1% weight of MWNT is compared with the pristine (*i.e.*, unfilled) epoxy matrix. Theoretical predictions using the Halpin–Tsai theory for the nanocomposite samples are also shown in the figure. The error in estimation of weight fraction for the various nanocomposite samples is estimated to be less than ±0.002%.

Quantum Hall Effect

- Integral Quantum Hall effect can be accurately modeled as a non-interacting electron gas in a magnetic field
- The Fractional Quantum Hall effect involves composite fermion quasi-particles which are electrons with attached flux quanta

Classical Hall Effect

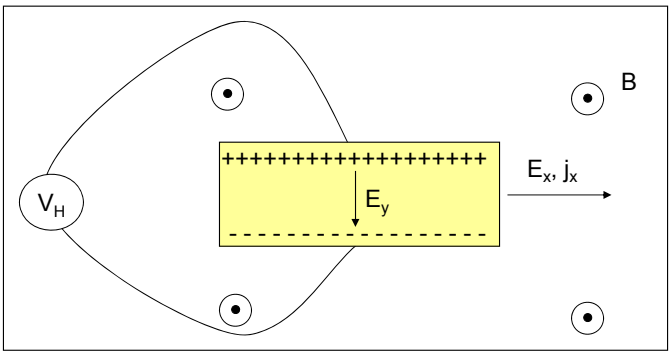

Experimental Values*

Metal	R_H (-1/nec)
Li	0.8
Na	1.2
Rb	1.0
Ag	1.3
Be	-0.2

$$E_y = -\left(\frac{\vec{v}}{c} \times \vec{B}\right)_y \longrightarrow R_H = \frac{E_y}{j_x B} = \frac{1}{nec}$$

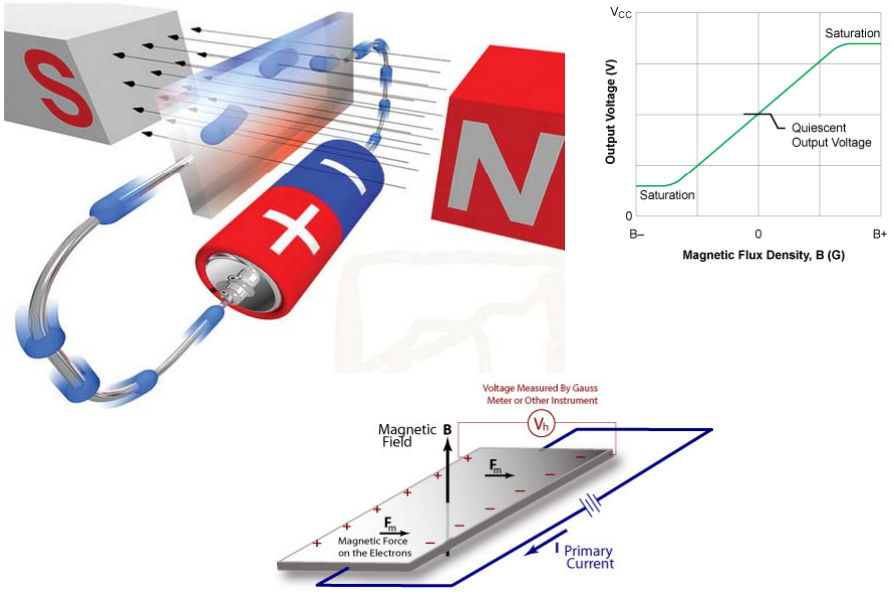

Integer QHE

Discovered in 1980,

Nobel Prize awarded to von Klitzing in 1985

$$\rho = \begin{bmatrix} 0 & -h/ie^2 \\ h/ie^2 & 0 \end{bmatrix}$$

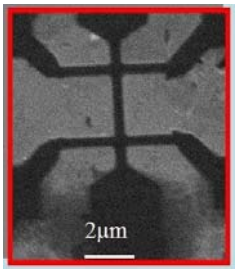

SEM image of a Hall bar*

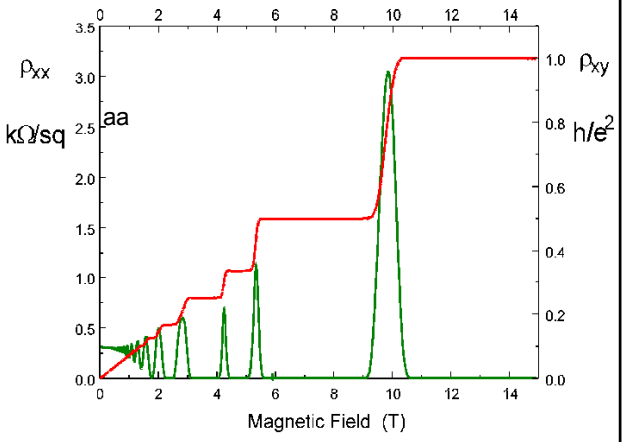

Quantum Mechanical Description

$$\hat{H}\psi = E\psi = \frac{1}{2m}(\hat{p} - \frac{e}{c}\hat{A})^2\psi$$

$$= \frac{1}{2m}\left[(p_x - eBy)^2 + p_y{}^2\right]\psi$$

Landau Gauge: $\hat{A} = -By\hat{x}$

$$\psi = e^{ik_x x}\phi(y) \longrightarrow H(e^{ik_x x}\phi) = \frac{\omega_c}{2}\left[-l^2\partial_y^2 + \left(\frac{y}{l} - lk_x\right)^2\right]e^{ik_x x}\phi = Ee^{ik_x x}\phi$$

$$l \equiv \left(\frac{\hbar c}{eB}\right)^{1/2}, \omega_c^2 = \frac{eB}{mc}$$

Degeneracy of Landau Levels

Each wavefunction is centered at $y = l^2 k_x$

$$0 < y < W \longrightarrow 0 < k_x < \frac{W}{l^2}, \quad k_x = \frac{2\pi}{L}n$$

$$0 < n < \frac{LW}{2\pi l^2}$$

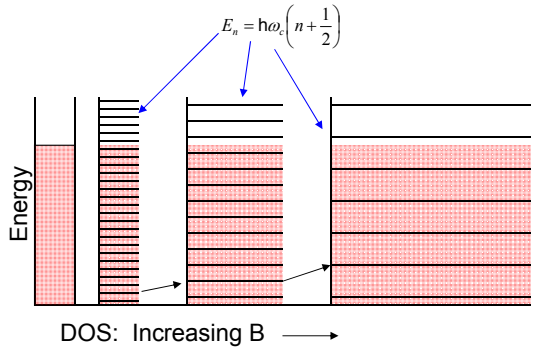

Impurity Effects

Isolated δ-fn potential localizes one extended state

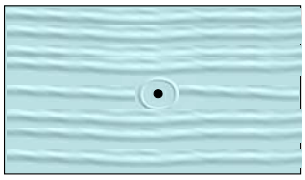

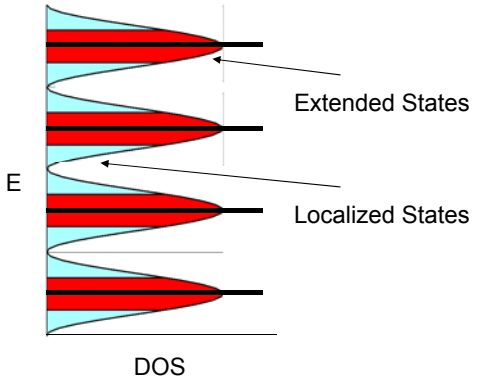

Only extended states carry current!

The Laughlin Argument for the Integer Hall effect

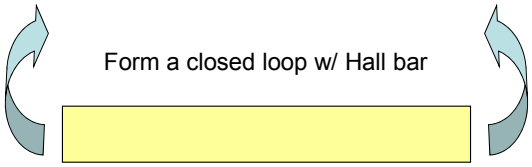

$$j_x = -\frac{\partial \langle H \rangle}{\partial A_x} \rightarrow I_x = -\frac{d\langle H \rangle}{d\Phi}$$

Change the flux through the loop by one quanta: $\Delta\Phi = \Phi_0 = \frac{h}{e}$

No change can take place in the bulk – move one electron to the other edge

$$\Delta\langle H \rangle = -pe[V(W) - V(0)]$$

$$I_x = p\frac{e^2}{h}(V_y) \rightarrow \sigma_{xy} = p\frac{e^2}{h}$$

p must be an integer

Fractional QHE

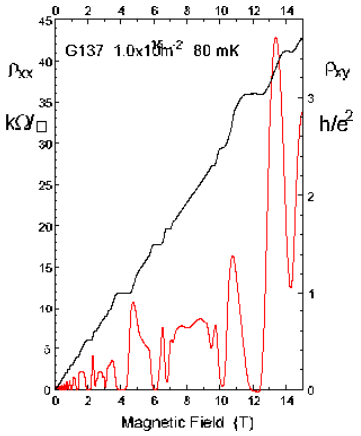

Filling factor is a rational fraction

$$\sigma_{xy} = \nu \frac{e^2}{h}, \nu = \frac{p}{q}$$

Cannot be explained in terms of free electrons

Composite Fermion Picture

Electrons ⟶ IQHE

Composite Fermions ⟶ FQHE

Fractional Hall effect encompasses states with filling factors: $\nu = \frac{\nu^*}{2p\nu^* \pm 1}$

Composite fermions can be viewed as electrons with attached flux quanta

$\vec{B}$ is screened to $\vec{B}^* = \vec{B} - 2pe\Phi_0$

Lowest Landau level splitting for composite fermions

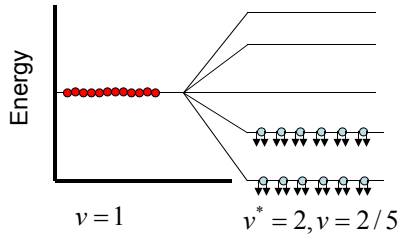

v=1 lowest Landau Level splits into levels separated by $\hbar\omega_c^*$

The fractional filling of electrons is really the integral filling of composite fermions

Vol 438|10 November 2005|doi:10.1038/nature04235 nature

LETTERS

Experimental observation of the quantum Hall effect and Berry's phase in graphene

Yuanbo Zhang[1], Yan-Wen Tan[1], Horst L. Stormer[1,2] & Philip Kim[1]

http://www.youtube.com/watch?v=bHo6_jltfc8

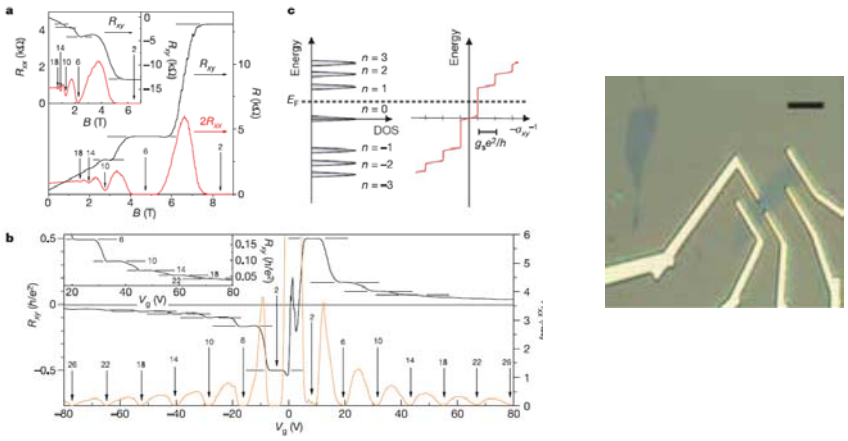

Figure 2 | Quantized magnetoresistance and Hall resistance of a graphene device. a, Hall resistance (black) and magnetoresistance (red) measured in the device in Fig. 1 at $T = 30$ mK and $V_g = 15$ V. The vertical arrows and the numbers on them indicate the values of B and the corresponding filling factor ν of the quantum Hall states. The horizontal lines correspond to $h/e^2\nu$ values. The QHE in the electron gas is shown by at least two quantized plateaux in R_{xy}, with vanishing R_{xx} in the corresponding magnetic field regime. The inset shows the QHE for a hole gas at $V_g = -4$ V, measured at 1.6 K. The quantized plateau for filling factor $\nu = 2$ is well defined, and the second and third plateaux with $\nu = 6$ and $\nu = 10$ are also resolved. **b,** Hall resistance (black) and magnetoresistance (orange) as a function of gate voltage at fixed magnetic field $B = 9$ T, measured at 1.6 K. The same convention as in **a** is used here. The upper inset shows a detailed view of high-filling-factor plateaux measured at 30 mK. **c,** A schematic diagram of the Landau level density of states (DOS) and corresponding quantum Hall conductance (σ_{xy}) as a function of energy. Note that, in the quantum Hall states, $\sigma_{xy} = -R_{xy}^{-1}$. The LL index n is shown next to the DOS peak. In our experiment the Fermi energy E_F can be adjusted by the gate voltage, and R_{xy}^{-1} changes by an amount $g_s e^2/h$ as E_F crosses a LL.

Observation of the fractional quantum Hall effect in graphene

Kirill I. Bolotin, Fereshte Ghahari, Michael D. Shulman, Horst L. Stormer & Philip Kim
Nature 462, 196–199 (2009)

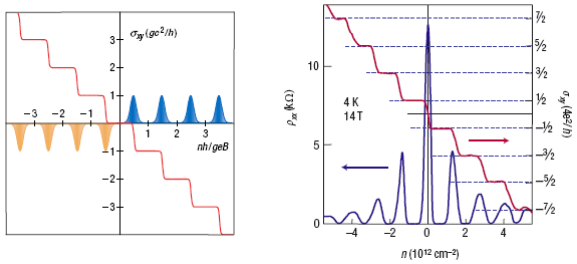

Comparison between conventional and unconventional integer QHE. (a) Schematic illustration of the conventional integer QHE in 2D semiconductor systems by showing the Hall conductivity versus the carrier density, where orange and blue peaks represent the density of state of Landau levels . **(b) The experimental** measurements of the Hall conductivity and longitudinal resistivity versus the carrier density in graphene .

K. S. Novoselov, et al. Nature Physics **2, 177 (2006).**
A. K. Geim, and K. S. Novoselov. Nature Materials **6, 183 (2007)**